

AD-A172 942

INVESTIGATION OF ION IMPLANTATION INTO HIGH PURITY AND  
CONTROLLABLY DOPED (U) SALFORD UNIV (ENGLAND DEPT OF  
ELECTRICAL ENGINEERING G CARTER 21 FEB 83

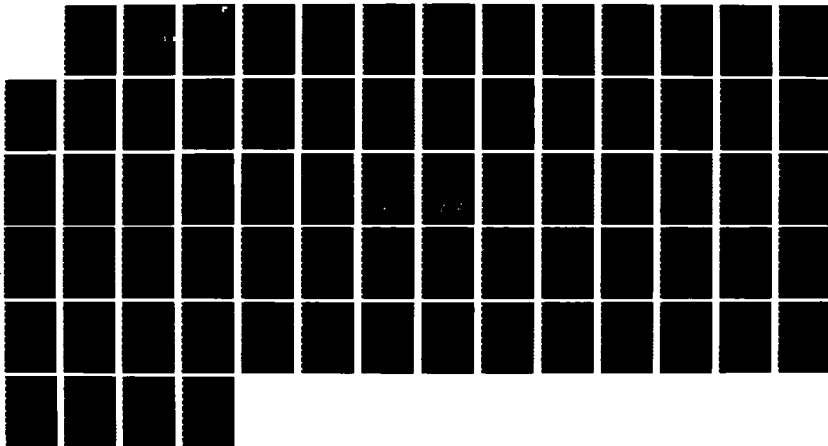
1/1

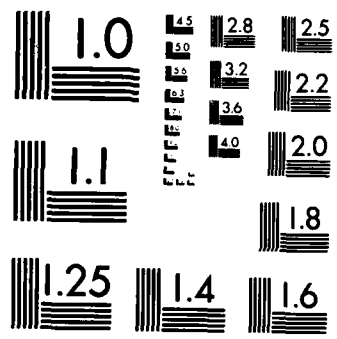
UNCLASSIFIED

AFWAL-TR-86-4111 F49620-82-C-0037

F/G 20/12

NL





MICROCOPY RESOLUTION TEST CHART  
NATIONAL BUREAU OF STANDARDS-1963-A

PHOTOGRAPH THIS SHEET

①

INVENTORY

AD-A172 942

DTIC ACCESSION NUMBER

INVESTIGATION OF ION  
IMPLANTATION INTO HIGH  
LEVEL PURITY AND CONTROLLABLY DOPED  
SILICON AND INTO GALLIUM ARSENIDE  
AFWAL-TR-86-4111

21 February 1983

DOCUMENT IDENTIFICATION

DISTRIBUTION STATEMENT A

Approved for public release;  
Distribution Unlimited

DISTRIBUTION STATEMENT

ACCESSION FOR	
NTIS	GRA&I <input checked="" type="checkbox"/>
DTIC	TAB <input type="checkbox"/>
UNANNOUNCED	<input type="checkbox"/>
JUSTIFICATION	
BY	
DISTRIBUTION /	
AVAILABILITY CODES	
DIST	AVAIL AND/OR SPECIAL
A-1	



DTIC  
ELECTE  
OCT 22 1986  
S D

DATE ACCESSIONED

DISTRIBUTION STAMP

DATE RETURNED

86 10 20 010

DATE RECEIVED IN DTIC

REGISTERED OR CERTIFIED NO.

PHOTOGRAPH THIS SHEET AND RETURN TO DTIC-DDAC



AFWAL-TR-86-4111

INVESTIGATION OF ION IMPLANTATION INTO HIGH PURITY AND CONTROLLABLY  
DOPED SILICON AND INTO GALLIUM ARSENIDE

G Carter  
Department of Electronic and Electrical Engineering  
University of Salford  
Salford M5 4WT  
UK

21 February 1983

Final Report for Period January 1982 - February 1983

Approved for Public Release; Distribution is Unlimited.

Prepared for:

UNITED STATES AIR FORCE  
Air Force Office of Scientific Research  
Building 410  
Bolling AFB, DC 20332  
U S A

EUROPEAN OFFICE OF AEROSPACE RESEARCH & DEVELOPMENT  
223/231 Old Marylebone Road  
London NW1 5th UK

MATERIALS LABORATORY  
Air Force Wright Aeronautical Laboratories  
Air Force Systems Command  
Wright-Patterson AFB, OH 45433

AD-A172 942

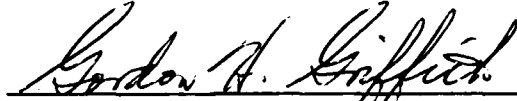
NOTICE

When Government drawings, specifications, or other data are used for any purpose other than in connection with a definitely related Government procurement operation, the United States Government thereby incurs no responsibility nor any obligation whatsoever; and the fact that the government may have formulated, furnished, or in any way supplied the said drawings, specifications, or other data, is not to be regarded by implication or otherwise as in any manner licensing the holder or any other person or corporation, or conveying any rights or permission to manufacture use, or sell any patented invention that may in any way be related thereto.


This report has been reviewed by the Office of Public Affairs (ASD/PA) and is releasable to the National Technical Information Service (NTIS). At NTIS, it will be available to the general public, including foreign nations.

This technical report has been reviewed and is approved for publication.

  
PATRICK M. HEMENGER  
Contract Monitor  
Laser & Optical Materials Branch

  
GORDON H. GRIFFITH, Acting Chief  
Laser & Optical Materials Branch  
Electromagnetic Materials Division

FOR THE COMMANDER



WILLIAM C. KESSLER, Acting Chief  
Electromagnetic Materials Division  
Materials Laboratory

If your address has changed, if you wish to be removed from our mailing list, or if the addressee is no longer employed by your organization please notify AFWAL/MLPO, W-PAFB, OH 45433 to help us maintain a current mailing list.

Copies of this report should not be returned unless return is required by security considerations, contractual obligations, or notice on a specific document.

REPORT DOCUMENTATION PAGE		READ INSTRUCTIONS BEFORE COMPLETING FORM
1. Report Number AFWAL-TR-86-4111	2. Govt Accession No. FY1457-82-03083	3. Recipient's Catalog Number
4. Title (and Subtitle) INVESTIGATION OF ION IMPLANTATION INTO HIGH PURITY AND CONTROLLABLY DOPED SILICON AND INTO GALLIUM ARSENIDE		5. Type of Report & Period Covered FINAL. JANUARY 1982-FEBRUARY 1983
		6. Performing Org. Report Number 2
7. Author(s) G CARTER		8. Contract or Grant Number F49620-82-C-0037
9. Performing Organization Name and Address DEPARTMENT OF ELECTRONIC AND ELECTRICAL ENGINEERING UNIVERSITY OF SALFORD SALFORD M5 4WT, UK		10. Program Element, Project, Task Area & Work Unit Numbers 61101F ILIR 00 88
11. Controlling Office Name and Address USAF, AFSC AIR FORCE OFFICE OF SCIENTIFIC RESEARCH BUILDING 410 BOLLING AFB DC 20332		12. Report Date FEBRUARY 1983
		13. Number of Pages 66
14. Monitoring Agency Name and Address AFWAL/MLPO Wright-Patterson AFB Oh 45433		15.
16. & 17. Distribution Statement Approved for public release; distribution unlimited.		
18. Supplementary Notes Also monitored by EOARD 223/231 Old Marylebone Rd. London NW1 5th, UK		
19. Key Words		
20. Abstract 1. Analytical analysis of the data derived from the use of Rutherford backscattering-channelling measurements of disorder production in ion implanted semiconductors for the determination of damage production mechanisms. 2. The redistribution and lattice incorporation of implanted impurities in Si during controlled furnace annealing to reorder the implantation damaged Si. 3. The production of disorder in InP by light and heavy ion implantation as a function of implant flux and fluence and implant temperature. 4. Investigation, in parallel with (3) of the damage creation and annealing processes associated with the interaction of the RBS/channelling analysis ion probe with heavy ion implantation damage in InP.		

## UNITED STATES AIR FORCE REPORT

### General Introduction

In the period since submission of the last report the grant sponsor has not required any analyses at Salford of materials developed at Wright Patterson AFB. Consequently, the period has been employed to conduct further back-up research relevant to the needs of the sponsors in-house programme. This study divides into four areas as follows:

1. Analytical analysis of the data derived from the use of Rutherford backscattering - channelling measurements of disorder production in ion implanted semiconductors for the determination of damage production mechanisms.
2. The redistribution and lattice incorporation of implanted impurities in Si during controlled furnace annealing to reorder the implantation damaged Si.
3. The production of disorder in InP by light and heavy ion implantation as a function of implant flux and fluence and implant temperature.
4. Investigation, in parallel with 3), of the damage creation and annealing processes associated with the interaction of the RBS/channelling analysis ion probe with heavy ion implantation damage in InP.

Substantial progress has been made in all four areas of study,

which are discussed separately and sequentially in the following report, and investigations in areas 1) and 2) have reached a satisfactory conclusion. Work in areas 3) and 4) is continuing at Salford, under alternative funding arrangements since USAF support is now terminated, because of the importance of understanding ion implantation processes in InP and related materials which have great potential application in opto-electronic devices.



## THE ANALYSIS OF RUTHERFORD SCATTERING-CHANNELLING MEASUREMENTS OF DISORDER PRODUCTION AND ANNEALING IN ION IRRADIATED SEMICONDUCTORS

Rutherford scattering and channelling of light probe ions (e.g.  $\text{He}^+$ ) has been extensively used for studies of disorder production in ion implanted semiconductors (1,2). The technique is employed to determine the number of lattice atoms displaced more than  $\sim 0.2 \text{ \AA}$  from equilibrium positions but unlike microscopic techniques does not give direct information about the nature of defects (although inferences can be made from dechannelling studies<sup>(3)</sup>), such as if the defects are isolated or in agglomeration as in amorphous zones. Study of the observed backscattering signal, either from fixed depth or depth integrated<sup>(2,4)</sup>, as a function of implant ion fluence, has however been used to infer, qualitatively, the nature of the disorder production process for a variety of energy deposition density conditions in Si<sup>(2)</sup> and GaAs<sup>(5)</sup> implanted at  $\sim 40 \text{ K}$  to minimise annealing processes. These processes range from simple defect accumulation until a sufficiently high local defect density is reached with increasing fluence that relaxation to amorphousness occurs<sup>(6,7)</sup> to direct impact amorphisation in individual cascades where defect densities are sufficiently large to cause instant collapse to amorphousness<sup>(8)</sup>. Various authors have analysed these<sup>(7)</sup> and composite extended models<sup>(9,10,11)</sup> of amorphousness accumulation and Carter and Webb<sup>(10,11)</sup> have indicated the general difficulties in assessing disorder production models from RBS/channelling studies if the production modes are complex and the manner in which the technique responds to different defect structures is unspecified. For less complex disorder production modes and by making reasonable assumptions about the technique response however, some insight into the form of backscattering yield - ion implant fluence functions can be obtained as is discussed in the present communication. It thus becomes possible to infer the importance of different disorder generation processes from RBS/channelling - ion

fluence studies. It will also be shown how simple annealing processes modify disorder accumulation and thus again how the operation of such processes may be inferred from RBS/channelling - ion fluence measurements.

For simplification and definiteness we assume that an implant ion may produce a completely amorphised area of solid  $a_a$  (at depth  $z$ ), and an area  $a_d$  which is disordered but not amorphised. If in further ion impact parts of the areas  $a_a$  or  $a_d$  produce further disorder in an already disordered but not amorphised area at depth  $z$ , the area of overlap is transformed to amorphousness. This is the single overlap model of earlier authors<sup>(7,9,10,11)</sup> and may readily be adapted to multiple overlap situations and where  $a_d$  is non discrete but composed of areas of variable disorder<sup>(10,11)</sup>. A set of coupled differential equations describing the fractions of area at depth  $z$ , amorphised  $A_a$ , disordered  $A_d$  and ordered  $A_u$  is readily developed and solved<sup>(7,9,10,11)</sup> as a function of ion fluence  $\phi$ .

Thus,

$$A_a = 1 - (1 + a_d \phi) \exp - (a_a + a_d) \phi \quad (1a)$$

$$A_d = a_d \phi \exp - (a_a + a_d) \phi \quad (1b)$$

and  $A_u = \exp - (a_a + a_d) \phi \quad (1c)$

where  $A_a + A_d + A_u = 1 \quad (1d)$

In RBS/channelling studies, the backscattering yield from depth  $z$  is composed of projectiles passing through the solid in a random direction scattering from all atoms and projectiles executing an aligned trajectory scattering from atoms displaced by  $\geq 0.2R$ <sup>(12)</sup>. Thus the yield  $Y_D$  from the partially amorphous, partially disordered and partially ordered crystal at depth  $z$ , compared to the yield from a totally amorphised solid  $Y_R$  is given by

$$Y_D/Y_R = A_a + A_d (1 - x) \frac{N_d}{N_s} + A_d x + A_u x \quad (2)$$

where  $x$  is the random fraction of the analysis beam at depth  $z$ ,  $N_d$  is the disorder density in disordered crystal and  $N_s$  the target density.

In equation (2) the atomic density of amorphised areas is assumed equal to that of the undamaged substrate. This is of course slightly incorrect and will lead to multiplication of the first term on the right hand side of equation (2) by a constant slightly less than unity. If  $N_{dc}$  is the critical local defect density to result in collapse to amorphousness then we may write  $\frac{N_{dc}}{N_s} = f$  as the critical fractional defect density to lead to collapse. Further if single overlap conditions are assumed then  $N_d = \frac{N_{dc}}{2}$ , and thus equation (2) may be rearranged using equation (1d), to give,

$$\frac{Y_D}{Y_R} = (1-x)A_a + (1-x)f/2 A_d + x \quad (3)$$

Substitution of equations (1a - 1c) into equation (3) leads to the result:

$$\frac{Y_D}{Y_R} = 1 - (1-x)\exp - (a_a + a_d)\phi + \{(1-x)(\frac{f}{2}-1) a_d \phi \exp - (a_a + a_d)\phi\} \quad (4)$$

Since the yield/fluence function is usually determined over several orders of magnitude in fluence,  $\phi$ , it is usual to plot<sup>(1,2)</sup> the  $\log Y_D/Y_R / \log \phi$  function and observe any features of the slope of this function<sup>(2,9,10)</sup>. It is readily deduced from equation (4) that this slope  $\frac{d(\log Y_D/Y_R)}{d \log \phi} = m$ .

$$= \phi \frac{\{(1-x)(a_a + a_d)\exp - (a_a + a_d)\phi + \{(1-x)(\frac{f}{2}-1)\} \{a_d - a_d(a_a + a_d)\phi\} \exp - (a_a + a_d)\phi\}}{\{1 - (1-x)\exp - (a_a + a_d)\phi + \{(1-x)(\frac{f}{2}-1)\} a_d \phi \exp - (a_a + a_d)\phi\}} \quad (5)$$

For small fluence,  $\phi$ , this equation may be expanded to

$$m = \phi \frac{\{(1-x)(a_a + a_d) + k a_d - k a_d (a_a + a_d)\phi\}}{-x + (a_a + a_d)\phi + k a_d \phi + \frac{1}{2}(a_a + a_d)^2 \phi^2} \quad (6)$$

where  $k = (1-x)(f/2-1)$ .

For small fluence, and consequently small disorder levels,  $x \ll 1$  and equation (6) becomes

$$m = 1 - \phi \frac{(a_a + a_d) + 2k a_d}{(a_a + a_d) + k a_d} \frac{1}{2} (a_a + a_d) \quad (7)$$

As fluence,  $\phi$ , tends to zero, the slope  $m$  tends to unity, typical of all disorder models and employing RBS/channelling analysis<sup>(10,11)</sup>.

We note some special cases of equation (7). First if direct impact amorphisation is the dominant disordering process than  $a_a \gg a_d$ , and as fluence increases, the slope always decreases from its initial value of unity. Such behaviour is observed with high energy density cascade processes<sup>(2,5)</sup>. Secondly, if disorder overlap processes are dominant then  $a_d \gg a_a$  and since  $k = f/2 - 1$ , then if  $f$  is a small fraction,  $k$  may be negative and the slope increases with fluence,  $\phi$ . This behaviour is observed with low energy density cascade processes<sup>(2,5)</sup>. At higher fluences the approximation of equation (7) becomes invalid and in all cases  $m$  finally tends to zero as  $\phi \rightarrow \infty$ . Thus low energy density cascades can lead to sigmoidal behaviour of the  $\log Y_D/Y_R/\log\phi$  function.

It is also interesting to note that departures from slope linearity may be expected to occur, from equation (7), when

$$\phi \frac{(a_a + a_d) + 2ka_d}{(a_a + a_d) + ka_d} (a_a + a_d) \approx 2 \quad (8)$$

For direct impact amorphisation dominance,  $a_a \gg a_d$ , this indicates  $\phi a_a \approx 2$ . If disorder accumulated linearly, without overlap of already amorphised regions, then  $\phi a_a \approx 1$  would be the saturation amorphous level, so that one concludes that linear slope is preserved up to a substantial fraction of complete amorphisation, as noted for high energy density cascades<sup>(2,5)</sup>. If disorder overlap dominates,  $a_d \gg a_a$ , then  $\phi a_d \approx \frac{f}{1-f}$  and again assuming linear accumulation as a guide, this indicates that departure from linearity occurs when the measured disorder level  $\frac{Y_D}{Y_R}$  is of order  $f/2$ . Thus if collapse to amorphousness occurs when the local defect density is of order 5-10%<sup>(3)</sup>, the backscattering yield/fluence function departs, on double logarithmic plot, from linearity when the measured disorder is at about this level. Thus the inference of Ref. 2 that superlinear behaviour of the  $\log Y_D/Y_R/\log\phi$  fluence function at about the 10% disorder level indicates a dominance of simpler defect production with subsequent amorphous collapse is shown to be valid.

Where the relative values of  $a_a$  and  $a_d$  are less well specified or more complex

models of disordering are assumed, the resulting predictions of the behaviour of the slope  $m$ , although analytically tractable lead to cumbersome results which are difficult to compare with experiment<sup>(10,11)</sup>. The present treatment for more clear cut cases does suggest, however, that useful indications of dominant disordering modes may be inferred from slope changes, and the disorder level at which they occur.

Finally, we note the complications which will arise from concurrent annealing processes, such as will occur during most non low temperature implantation of semi-conductors<sup>(2)</sup>. For brevity we will specify the form of disorder production as direct impact amorphisation alone and consider a first order annealing process described by a single time constant  $\tau$  (which will be temperature dependent). The rate equation for amorphousness production is then

$$\frac{dA_a}{dt} = Ja_a (1-A_a) - \frac{A_a}{\tau} \quad (9a)$$

where  $J$  is the ion flux density.

This equation may be rewritten in terms of ion fluence  $\phi$  as

$$\frac{dA_a}{d\phi} = a_a \left\{ 1 - A_a \left( 1 + \frac{1}{a_a J \tau} \right) \right\} \quad (9b)$$

which solves to

$$A_a = \left\{ \frac{a_a J \tau}{1 + a_a J \tau} \right\} \left\{ 1 - \exp - \left( \frac{1 + a_a J \tau}{a_a J \tau} \right) a_a \phi \right\} \quad (9c)$$

The RBS/channelling yield will be approximately proportional to this area, and so it is readily deduced that the low fluence slope,  $m$ , of the  $\log Y_D/Y_R/\log \phi$  function is

$$m \approx 1 - \phi \cdot a_a \left( 1 + \frac{1}{a_a J \tau} \right) \quad (10)$$

Just as for the previous cases considered, the very low fluence slope is unity and, as for the non-annealing, direct impact amorphisation case, the slope  $m$  decreases with increasing fluence  $\phi$ . The faster the annealing process (smaller  $\tau$ ) the lower the fluence (and associated disorder level) at which reduction below unity slope occurs. The larger the ion flux density, the larger the disorder level at which reduction

below unity slope occurs. It is thus partly clarified why comparisons<sup>(2)</sup> of Ar ion implantation of Si at 40 K and at 300 K lead to a reduced log disorder - log fluence slope at the higher temperature at all fluences. In this case however some disorder accumulation process probably occurs also, so that the full analysis is rather more complex than the above. In such cases the details of the disorder-fluence behaviour depend sensitively on the model assumptions<sup>(13)</sup> and if both disordering and annealing processes are complex, so also is the behaviour of the slope  $m$ . If, however, low temperature studies suggest dominance of direct impact amorphisation, then higher temperature studies and variable flux density studies will allow estimation of the annealing time constant,  $\tau$ , if single valued, from observation of the stages at which  $m$  departs from unity for different flux densities.

It should also be noted that, as a further indication of annealing processes, the saturation disorder level, as predicted from equation (9c) is an increasing function of flux density and a decreasing function of temperature (decreasing  $\tau$ ).

It is thus clear that study of RBS/channelling results of log (yield) as a function of log (implant fluence) can be used to distinguish probable disordering mechanisms, to estimate disorder densities required for amorphousness collapse and to investigate thermal annealing processes. As noted earlier more complex model assumptions (10,11,13) can be treated similarly but with less clarity of prediction.

#### References

1. R S Walker and D A Thompson. Rad Effects 37, 113 (1978) and D A Thompson and R S Walker. Rad Effects 36, 91 (1978).
2. D A Thompson, A Golanski, H K Haugen, D V Stevanovic, G Carter and C E Christodoulides. Rad Effects 52, 69 (1980).
3. M L Swanson, L M Howe, T E Jackman and J A Moore. Nucl Instrum & Meth 194, 165 (1982).
4. C E Christodoulides, N J Kadhim and G Carter. Rad Effects 52, 225 (1980).
5. N P Tognetti, G Carter, D V Stevanovic and D A Thompson. Rad Effects. To be published, 1982.
6. M L Swanson, J R Parsons and C W Hoelke. 'Radiation Effects in Semiconductors' (Eds. Corbett and Watkins, Gordon & Breach Ltd, London) p359 (1971).
7. J F Gibbons. Proc IEEE 60, 1062 (1972).
8. F F Morehead and B L Crowder. Rad Effects 6, 25 (1970).

9. J R Dennis and E B Hale. J Appl Phys 49, 119 (1978).
10. G Carter and R P Webb. Rad Effects Letters 43, 19 (1979).
11. R P Webb and G Carter. Rad Effects 42, 159 (1979).
12. E Bøgh. Can J Phys 46, 653 (1968).
13. R P Webb and G Carter. Rad Effects. To be published, 1982.

## EPITAXIAL RECRYSTALLISATION OF GALLIUM IMPLANTED (100) SILICON

### ABSTRACT

High depth resolution Rutherford backscattering/channelling and low angle X-ray texture camera analysis have been employed to study the recrystallisation behaviour of gallium implanted (100) silicon during low temperature furnace annealing at 465°C.

The recrystallisation behaviour was found to depend strongly on the gallium concentration, exhibiting three distinct recrystallisation regimes.

For low fluence gallium implants peak concentration  $\sim 0.3$  atomic percent, epitaxial recrystallisation was observed to proceed to completion with a substantial fraction of the implanted gallium being incorporated on to substitutional lattice sites. The epitaxial recrystallisation rate was enhanced by gallium concentrations  $\gtrsim 0.2$  atomic percent and substitutional concentrations in excess of the maximum equilibrium value were observed. In addition, X-ray analysis implies the existence of a thin,  $\lesssim 5$  nm, preferentially oriented polycrystalline surface layer after annealing.

For higher gallium fluences, peak concentration  $\sim 1.8$  atomic percent epitaxial recrystallisation no longer proceeded to completion but ceased some 20 nm from the silicon surface. Considerable gallium was observed to be redistributed towards the surface by the advancing crystal-amorphous interface and the epitaxial recrystallisation rate was again observed to be enhanced by gallium concentrations  $\lesssim 0.2$  atomic percent, reaching a maximum value of 7.5 times that of undoped amorphous silicon layers. Substitution gallium concentrations  $\sim 3.0 \times 10^{20}$  Ga/cm<sup>3</sup> were observed, a value comparable to that measured following pulsed laser annealing.



Finally, X-ray analysis confirms that the 20 nm surface region contains preferentially aligned polycrystallites.

For the highest gallium fluences investigated, peak concentration  $\sim 4.0$  atomic percent epitaxial recovery was initially slow and extensive gallium redistribution was observed after  $\sim 15$  minutes annealing. X-ray analysis again confirmed the presence of preferentially oriented polycrystallites.

## INTRODUCTION

A thin amorphous silicon layer can be produced on a single crystal silicon substrate by high fluence ion irradiation. Such layers are metastable and recrystallise epitaxially from the underlying substrate when heated to temperatures around  $450^{\circ}\text{C}$ <sup>1</sup>. The epitaxial regrowth kinetics of uncontaminated layers have been investigated in detail and the recrystallisation process is observed to be thermally activated with a well defined activation energy<sup>1,2,3</sup>.

The activation energy is observed to be a constant for all crystal orientations but the regrowth velocity is orientation dependent, being twenty-five times faster in the  $\langle 100 \rangle$  direction than in the  $\langle 111 \rangle$  direction at  $550^{\circ}\text{C}$ <sup>4</sup>. Thermodynamic arguments and modelling of the amorphous-crystal interface have led to a reasonable understanding of the recrystallisation process and its orientation dependence<sup>5</sup>. The recrystallisation interface is believed to break up into terraced (111) planes, the number of terraces being determined by the angle the regrowth plane subtends to the (111) surface. Epitaxial recrystallisation is then thought to proceed via the growth of  $\langle 110 \rangle$  ledges on this terraced interface. The orientation dependent regrowth velocity then simply reflects the ledge concentration (or more particularly the kink concentration).

In addition to orientation dependence the epitaxial recrystallisation velocity of silicon displays a strong dependence on the type and concentration of impurities present during regrowth. Low concentrations ( $\sim 0.5$  atomic percent) of certain impurities are observed to enhance or retard the epitaxial regrowth velocity by up to an order of magnitude. Initial investigations by Csepregi et al<sup>6,7</sup>, suggested that electrically active (B,P,As) impurities were responsible for enhancing epitaxy while electrically inactive species (N,O,C)

retarded it.

More recent data by Suni et al<sup>8</sup> and Lietoila et al<sup>3</sup> supports the view that it is the electronic properties of the impurity which determines the rate of epitaxy. A model for this behaviour has recently been proposed by Williams and Elliman<sup>9</sup>.

For high impurity concentrations (> solubility limit) epitaxial regrowth is considerably more complex and both electrically active and inactive species are observed to retard epitaxy<sup>10,11</sup>. In cases where epitaxy is able to proceed impurity redistribution often results as a consequence of segregation at the advancing amorphous-crystal interface, and in extreme cases epitaxy completely ceases and polycrystallite nucleation may ensue<sup>11</sup>.

To understand the role of impurities in the recrystallisation kinetics of silicon it is essential to establish a data base of information from which comparisons and patterns can be explored. At present detailed recrystallisation kinetics exists only for a few species and consequently it is difficult to correlate observations and theoretical predictions. This paper presents the results of a detailed investigation into the recrystallisation behaviour of gallium implanted (100) silicon. Regrowth kinetics and impurity redistribution are examined in detail as a function of gallium concentration in the range up to 4.0 atomic percent.

#### EXPERIMENTAL

High depth resolution Rutherford backscattering (RBS) and channelling of 2 MeV He<sup>+</sup> was used in conjunction with X-ray texture camera analysis to characterise the recrystallisation behaviour of gallium implanted (100) silicon during annealing at 465°C

Commercially prepared, float zone (100) silicon substrates with low bulk impurity concentrations ( $>100 \text{ k}\Omega \text{ cm}$ ) were employed throughout this investigation. All samples were chemically cleaned and the native oxide removed just prior to implantation. During implantation the target chamber pressure was maintained at  $\sim 10^{-7}$  torr and samples were cooled to  $\sim 150 \text{ K}$  by a liquid nitrogen cold finger. All samples were tilted  $7^\circ$  from the incident beam direction to minimize ion channelling effects and all implants were performed with  $40 \text{ kV Ga}^+$  ions.

Post implant annealing was carried out in a quartz tube furnace with a flowing atmosphere of  $85\% \text{ N}_2$  and  $15\% \text{ H}_2$ . The furnace temperature was profiled with a Ni/Cr : Ni/Al thermocouple and samples were always positioned within the accurately determined constant temperature zone. Minimum anneal times of 10 minutes were employed to reduce the anneal time uncertainty due to warm up and cool down periods.

RBS and channelling measurements were performed with  $2 \text{ MeV He}^+$  and a solid state detector ( $15 \text{ keV fwhm}$ ) was employed in a low angle exit geometry to provide an absolute depth resolution of  $\sim 80 \text{ \AA}$ <sup>12</sup>. The actual scattering geometry employed is depicted inset in subsequent figures. RBS depth scales were determined from the semi-empirical stopping powers of Ziegler and Chu<sup>18</sup> and gallium concentrations were determined by assuming a constant atomic density of  $5 \times 10^{22} \text{ cm}^{-3}$  for silicon.

X-ray analysis was performed with a low angle cylindrical texture camera<sup>13,14</sup> employing Cu-K $\alpha$  radiation. The collimated X-ray beam was incident at  $12^\circ$  to the sample surface to sample shallow surface layers. The geometry of the camera was such that the X-ray beam was coaxial with the cylinder axis and the sample was positioned at the centre of the cylinder on a rotating shaft.

## RESULTS AND DISCUSSION

As outlined above the epitaxial recrystallisation process is well characterised for uncontaminated amorphous silicon layers and a reasonable understanding of the recrystallisation mechanism is emerging. For contaminated layers however, the available experimental data is limited and consequently the physical understanding of impurity effects is less complete.

The present discussion examines the recrystallisation kinetics of gallium implanted (100) silicon during thermal annealing at 465°C. The results for low ( $6 \times 10^{14}$  Ga/cm<sup>2</sup>), medium ( $3.2 \times 10^{15}$  Ga/cm<sup>2</sup>) and high ( $7.5 \times 10^{15}$  Ga/cm<sup>2</sup>) fluence gallium implants are summarised in figures 1, 2 and 3 respectively. The top half of each figure depicts the as implanted (full curve) and post anneal (broken curve) gallium distributions with the final substitutional gallium distribution indicated by the shaded area of the curve. The lower portion of each figure depicts the regrowth process of the amorphous-crystal interface for isothermal annealing at 465°C. It should be noted that the terms low, medium and high fluence referred to above are arbitrary. They have only been employed to simplify the following discussion and refer to the implants reported in figures 1-3.

For the low dose implant, figure 1, epitaxial regrowth is observed to redistribute a small fraction (~ 13%) of the implanted gallium towards the silicon surface. The peak gallium concentration is reduced from ~ 0.3 to ~ 0.25 atomic percent and the final distribution is observed to have a narrow gallium peak at or near the silicon surface. The width of this peak is within the RBS system resolution and its exact height and depth distribution cannot be extracted from the data. Observation of the gallium distribution as a function of anneal time shows that gallium is redistributed by the advancing recrystallisation front, as previously reported for indium implanted

silicon<sup>11</sup>. This form of redistribution is commonly observed for impurity concentrations above the equilibrium solubility limit and it has been speculated that interfacial stress is the driving force for the redistribution<sup>11</sup>. During regrowth a high fraction of the implanted gallium is incorporated on to substitutional lattice sites and a peak substitutional gallium concentration of  $\sim 1 \times 10^{20}$  Ga/cm<sup>3</sup> is measured after regrowth. This value is  $\sim 2.5$  times greater than the maximum equilibrium substitutional solubility of gallium in silicon ( $4 \times 10^{19}$  Ga/cm<sup>3</sup>)<sup>15</sup>.

From the lower half of figure 1 the average epitaxial regrowth rate of silicon is observed to be enhanced by the presence of low gallium concentrations. The average regrowth rate for the case shown in figure 1 is 0.28 nm/min, compared to  $\sim 0.20$  nm/min for undoped amorphous silicon. The regrowth rate is clearly concentration dependent, reaching its peak value of 0.55 nm/min at the peak of the gallium distribution. For gallium concentrations below  $\sim 0.2$  atomic percent the regrowth rate remains essentially at the undoped level of  $\sim 0.2$  nm/min while for concentrations above this value the rate increases significantly, remaining approximately constant throughout the broad peak in the gallium distribution. The regrowth rate finally slows again as the recrystallisation front passes through the gallium peak and approaches the silicon surface. From figure 1 it is clear that epitaxial recrystallisation approaches completion after annealing at 465°C for 180 minutes. Final Rutherford backscattering analysis suggests that the recrystallised layer is near perfect crystal as shown in figure 4. This matter will be discussed later with regard to X-ray texture camera analysis. It should be noted that the maximum regrowth rate of 0.55 nm/min observed above is approximately three times that observed for undoped amorphous layers, an enhancement which is similar to that observed by Csepregi et al<sup>6</sup> for 0.22 atomic percent phosphorus impurity during annealing at 475°C.

6

The regrowth behaviour for medium gallium concentrations, up to  $\sim 1.8$  atomic percent, is depicted in figure 2. From the upper half of the figure it is apparent that considerable gallium redistribution occurs during regrowth. Redistribution is far more extensive than that observed for lower gallium concentrations and the final gallium distribution has a broad maximum distributed over  $\sim 20$  nm at the silicon surface. Redistribution is again observed to occur at the recrystallisation interface but the redistribution peak broadened rapidly towards the surface during the final anneal. Impurity redistribution of this kind is generally indicative of polycrystallite grain boundaries and hence this data suggests that the surface region of the silicon sample is no longer amorphous but polycrystalline. This is supported by X-ray texture camera analysis as discussed later. During regrowth the initial peak gallium concentration of  $\sim 1.8$  atomic percent is reduced to  $\sim 1.0$  atomic percent, a 44% reduction, which is considerably more than the 23% reduction observed for the lower dose sample. Following recrystallisation a large fraction of the implanted gallium is again observed to reside on substitutional lattice sites. The peak substitutional concentration of  $3.0 \times 10^{20}$  Ga/cm<sup>3</sup> is 7.5 times the maximum equilibrium solubility of gallium in silicon, a value which is comparable to that achieved by liquid phase epitaxy during pulsed laser annealing<sup>16</sup>,  $\sim 4 \times 10^{20}$  Ga/cm<sup>2</sup>. Comparison of figures 1 and 2 shows that redistribution commences at a similar gallium concentration in both cases.

From the lower portion of figure 2 the average regrowth velocity is again observed to be significantly enhanced by the presence of gallium. The average regrowth velocity of 0.7 nm/min is 3.5 times that expected for uncontaminated layers and the maximum velocity of  $\sim 1$  nm/min is a factor of 5 times that of uncontaminated layers. As with the low dose implant epitaxial regrowth proceeds at near the undoped level for gallium

concentration below  $\sim 0.2$  atomic percent and then increases with increasing gallium concentration for concentrations above this value. It is also apparent from the regrowth behaviour depicted that epitaxial recrystallisation does not proceed to completion for this sample but ceases  $\sim 20$  nm from the surface. This is consistent with the formation of a polycrystalline surface layer as suggested above. Similar behaviour has previously been reported for indium implanted (100) silicon during thermal annealing at  $525^{\circ}\text{C}$ <sup>17</sup>. The conditions under which a polycrystalline layer will form are difficult to predict since the nucleation of such layers is a function of the regrowth velocity, the substrate temperature and the type and concentration of impurity, and many of these parameters are interrelated.

The anneal behaviour of a high fluence gallium implant  $7.5 \times 10^{15}$  Ga/cm<sup>2</sup>, is depicted in figure 3. Comparison of the as-implanted and post anneal gallium distributions shows that significant bidirectional redistribution of gallium has occurred during the total anneal time of 45 minutes at  $465^{\circ}\text{C}$ . The form and the extent of the gallium redistribution is inconsistent with an epitaxial regrowth process and it again suggests the presence of polycrystallite grain boundaries. The extent and the bidirectional nature of the redistribution suggest that polycrystallites exist throughout the region of the originally amorphous layer. It should be noted that little or no gallium redistribution was observed during the first 15 minutes of the anneal but after this initial period redistribution occurred rapidly. Fletcher et al<sup>17</sup> have also noted the formation of an extensive polycrystalline layer for high indium concentrations in (100) silicon during annealing at  $500^{\circ}\text{C}$ .



The regrowth behaviour depicted in the lower half of figure 3 confirms that epitaxy is far from complete. The regrowth rate is observed to be severely retarded ( $\sim 0.15$  nm/min) by the presence of high gallium concentration and comparison with figure 2 suggest that interfacial gallium concentrations in the range 1-2 atomic percent are sufficient to allow polycrystallite nucleation. Whether the polycrystallite nucleation is a consequence of retarded epitaxy or of gallium concentration cannot be deduced from this data.

Figure 4 summarises the extent of epitaxial recovery for the low, medium and high dose implants of figures 1, 2 and 3. The upper half of the figure shows Rutherford backscattering spectra for samples as-implanted and after anneal. The extent of epitaxial recovery is plotted in the lower half of the figure along with the fraction of implanted gallium residing on substitutional lattice sites after annealing.

Following the final anneal stage each annealed sample was examined in a cylindrical X-ray texture camera to establish the nature of the annealed surface layer. X-ray analysis was performed on samples as removed from the furnace and after removing the thin native oxide ( $\lesssim 5$  nm) which had developed throughout analysis. The oxide was observed to contribute to the diffraction pattern and to avoid confusion only the results for etched samples are presented here. X-ray texture camera results are reproduced in figures 5 and 6. Figure 5a shows the diffraction pattern obtained from crystalline silicon for comparison and figures 5b, 6a and 6b, show the results obtained for the low, medium and high dose samples discussed above. For the camera geometry employed in this study<sup>13,14</sup>, the vertical axis of the photographs as displayed, represents variable  $2\theta_B$ , where  $\theta_B$  is the Bragg angle of the reflection. Horizontal bands of uniform intensity thus represents scattering from randomly oriented planes or polycrystals.

Horizontal lines of variable intensity imply polycrystallites of preferred crystallographic orientation.

Comparison of figures 5a, 5b, 6a and 6b clearly suggests that preferentially oriented polycrystallites exist in each of the implanted and post annealed samples. The intensity of the polycrystal bands, although not accurately reproduced here, is observed to increase as the extent of epitaxial recovery, as shown in figure 4, decreases. Thus the increasing intensity probably reflects the extent of the polycrystal layer. It is interesting to note that the orientation of the crystallites is the same in all cases independent of the extent of the polycrystal layer. This, along with the fact that a preferred orientation exists, suggests that the polycrystalline layer is nucleated from the amorphous-crystal interface.

A particularly surprising outcome of the X-ray analysis is the existence of preferentially oriented polycrystals in the lowest dose sample. The RBS spectrum of this sample shown in figure 4, suggests complete epitaxial recover, highlighting the insensitivity of the RBS/channelling technique to certain crystal defects.

#### SUMMARY AND CONCLUSIONS

The Rutherford backscattering/channelling technique has been combined with X-ray texture camera analysis to characterise the recrystallisation behaviour of gallium implanted (100) silicon during furnace annealing at 465°C.

For peak gallium concentrations  $\lesssim 0.3$  atomic percent the RBS/channelling technique suggests that epitaxial recrystallisation proceeds to completion with a substantial fraction of the implanted gallium being incorporated onto substitutional lattice sites. The epitaxial recrystallisation rate is enhanced by the presence of these low gallium concentrations and is observed

to increase with increasing concentration for concentrations  $\gtrsim 0.2$  atomic percent. During epitaxial recovery a small fraction (13%) of gallium is redistributed by the advancing amorphous-crystal interface. The gallium incorporated into the recrystallised layer is highly substitutional with a peak substitutional concentration 2.5 times the maximum equilibrium solubility limit. RBS/channelling analysis suggests that epitaxy is complete but X-ray texture camera analysis implies the existence of a very thin preferentially oriented polycrystalline layer. Comparison of the RBS spectra and the X-ray data further suggests that this layer is  $\lesssim 5$  nm thick.

When the peak gallium concentration is increased to  $\sim 1.8$  atomic percent epitaxial recrystallisation no longer proceeds to the near surface region but ceases some 20 nm from the silicon surface. In the region where epitaxial recrystallisation occurs the regrowth rate is again observed to be enhanced by the presence of gallium concentrations  $\gtrsim 0.2$  atomic percent, despite the fact that much of the implanted gallium is redistributed by the amorphous-crystal interface. Gallium incorporated into the regrown silicon layer is highly substitutional and a peak substitutional concentration 7.5 times the maximum equilibrium solubility limit was observed, a value which is comparable to that observed following pulsed laser annealing. Gallium redistribution within the 20 nm surface region suggests the existence of polycrystal grain boundaries. X-ray texture camera analysis confirms this and further shows that the polycrystallites are preferentially oriented.

When the fluence of 40 keV gallium is increased to  $7.5 \times 10^{15}$  Ga/cm<sup>2</sup>, a peak gallium concentration of  $\sim 4.0$  atomic percent, annealing at 465°C results in little epitaxial recrystallisation. Epitaxy proceeds for  $\sim 5$  nm during which the regrowth rate is severely retarded. The gallium distribution is observed to remain approximately Gaussian during the first 15 minutes at

1

465° and then it rapidly redistributes both towards the silicon surface and towards the original amorphous-crystal interface. This rapid redistribution is again consistent with grain boundary diffusion and X-ray analysis again confirms the existence of preferentially oriented crystallites.

#### ACKNOWLEDGEMENTS

The authors are grateful to USAF for provision of a research grant which enabled the prosecution of this study and to NATO for provision of a research grant which enabled discussion of the investigation with Dr D A Thompson and colleagues at McMaster University (Canada).

REFERENCES

- 1) L Csepregi, J W Mayer and T W Sigmon.  
Phys Lett 54A, 157 (1975).
- 2) B Drosd and J Washburn.  
J Appl Phys 51, 4106 (1980).
- 3) A Lieloila, A Wakita, T W Sigmon and J F Gibbons.  
J Appl Phys 53, 4399 (1982).
- 4) L Csepregi, E F Kennedy and J W Mayer.  
J Appl Phys 49, 3906 (1978).
- 5) F Spaepen and D Turnbull.  
In "Laser and Electron Beam Processing of Semiconductor Structures",  
Chapter 3. (J M Poate and J W Mayer, Eds.). Academic Press, NY.
- 6) L Csepregi, E F Kennedy, T J Gallagher, J W Mayer and T W Sigmon.  
J Appl Phys 48, 4234 (1977).
- 7) E F Kennedy, L Csepregi, J W Mayer and T W Sigmon.  
J Appl Phys 48, 4241 (1977).
- 8) I Suni, G Goltz, M G Grimaldi, M-A Nicolet and S S Lau.  
Appl Phys Lett 40, 269 (1982).
- 9) J S Williams and R G Elliman.  
To be published, Phys Rev Lett.
- 10) J S Williams and R G Elliman.  
Appl Phys Lett 37, 829 (1980).
- 11) J S Williams and R G Elliman.  
Nucl Instr Meth 183, 758 (1981).
- 12) J S Williams.  
Nucl Instr Meth 149, 207 (1978).
- 13) C A Wallace and R C C Ward.  
J Appl Cryst 8, 255 (1975).
- 14) C A Wallace and R C C Ward.  
J Appl Cryst 8, 545 (1975).
- 15) F A Trumbore.  
Bell Syst Tech J 39, 205 (1960).
- 16) C W White, S R Wilson, B R Appleton, F W Young and J Narayan.  
In "Laser and Electron Beam Processing of Materials". (C W White  
and P S Peercy, Eds.). Academic Press, NY.
- 17) J Fletcher, J Narayan and D W Holland.  
In "Microscopy of Semiconductor Materials 1981". (A G Cullis and  
D C Joy, Eds.), (1981).
- 18) J F Zeigler and W K Chu.  
At Data Nucl Data Tables 13, 481 (1974).

FIGURE CAPTIONS

- Figure 1: (a) Gallium distribution as obtained from RBS analysis of as-implanted (full curve) and post annealed gallium implanted (100) silicon samples.  
(b) Amorphous layer recovery as a function of anneal time at 465°C. Dotted line shows regrowth rate of undoped amorphous silicon.  $3.2 \times 10^{15}$
- Figure 2: Gallium distribution and regrowth kinetics as described in Figure 1.  
Implant: 40 keV,  $7.5 \times 10^{15}$  Ga/cm<sup>2</sup>.
- Figure 3: Gallium distribution and regrowth kinetics as described in Figure 1.  
Implant: 40 keV,  $6 \times 10^{14}$  Ga/cm<sup>2</sup>.
- Figure 4: (a) Channelled RBS spectra as-implanted and following final anneal for  $6 \times 10^{14}$  Ga/cm<sup>2</sup> - O,  $3.2 \times 10^{15}$  Ga/cm<sup>2</sup> - Δ, and  $7.5 \times 10^{15}$  Ga/cm<sup>2</sup> - □ implants.  
(b) Amorphous layer recovery and substitutional gallium fraction as a function of gallium fluence.
- Figure 5: X-ray texture camera diffraction patterns for pure crystalline silicon (top) and for the sample examined in Figure 1 after final anneal (bottom).
- Figure 6: X-ray texture camera diffraction patterns for the sample examined in Figure 2 (top) and Figure 3 (bottom) after final anneal.

Epitaxial regrowth of Gallium implanted Silicon,  
medium Gallium concentration.

$3.2 \times 10^{15} / \text{cm}^2$

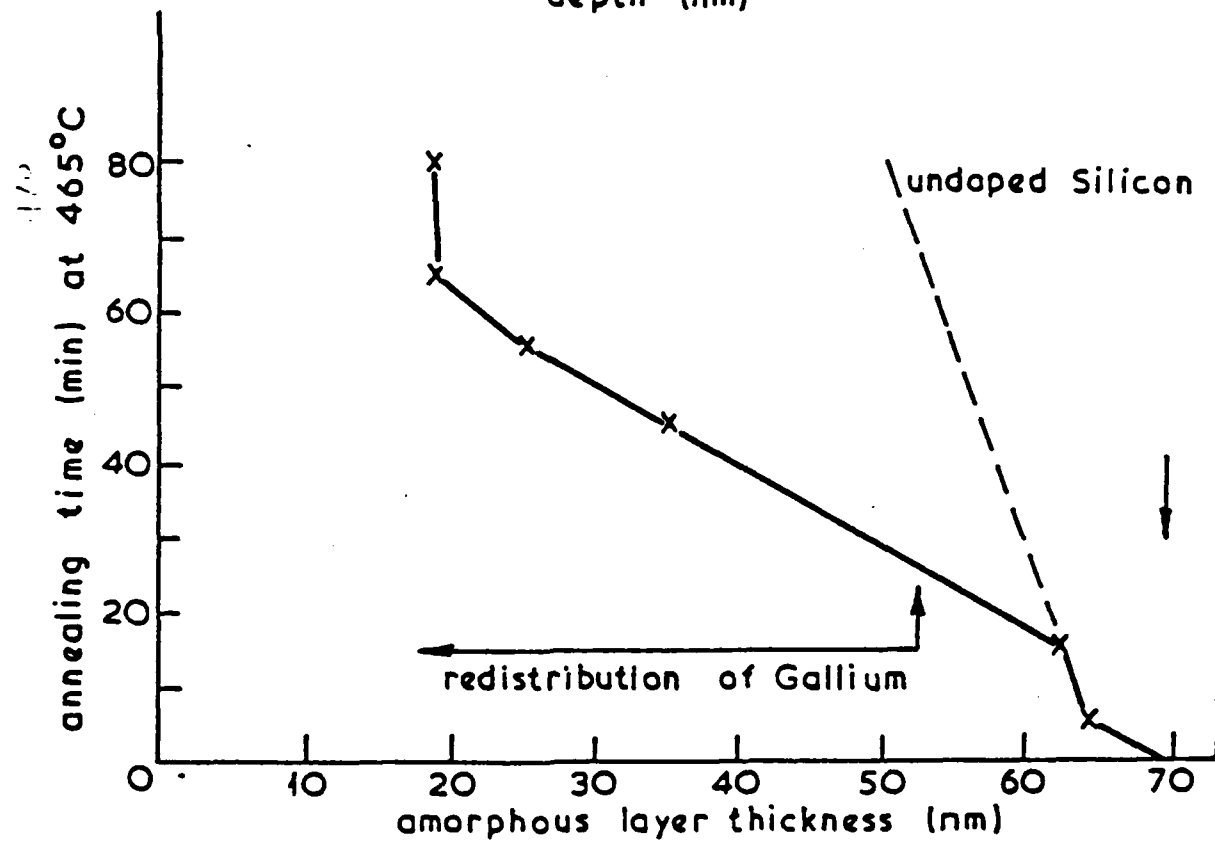
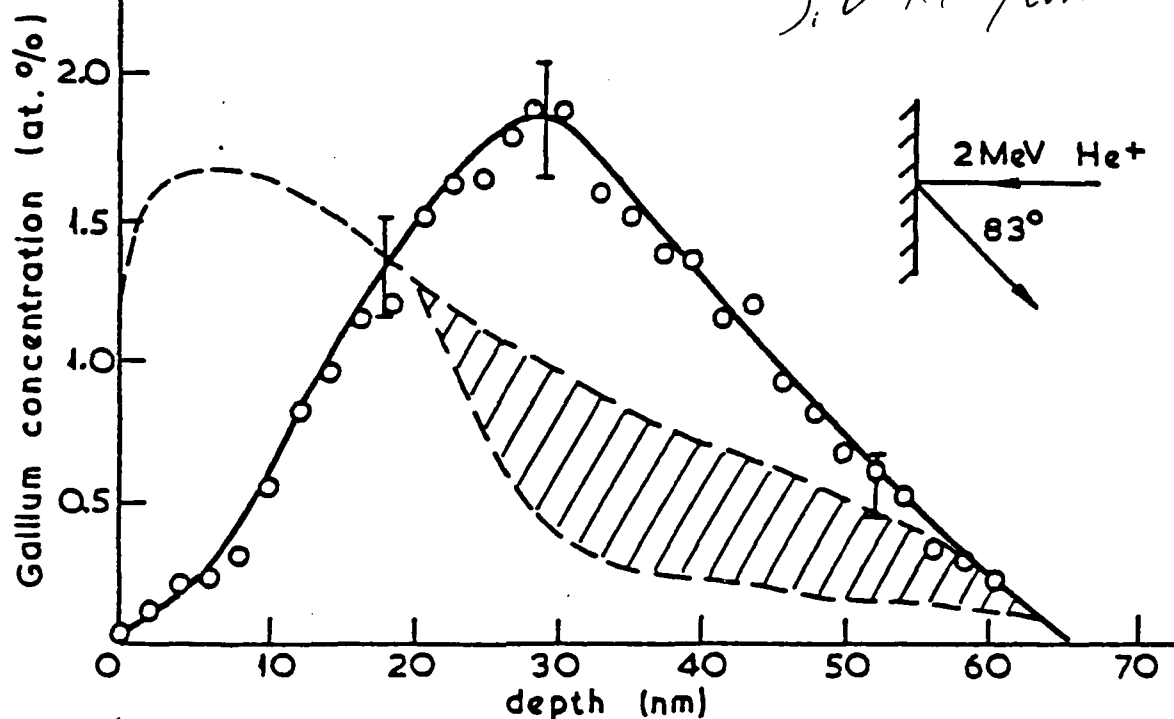
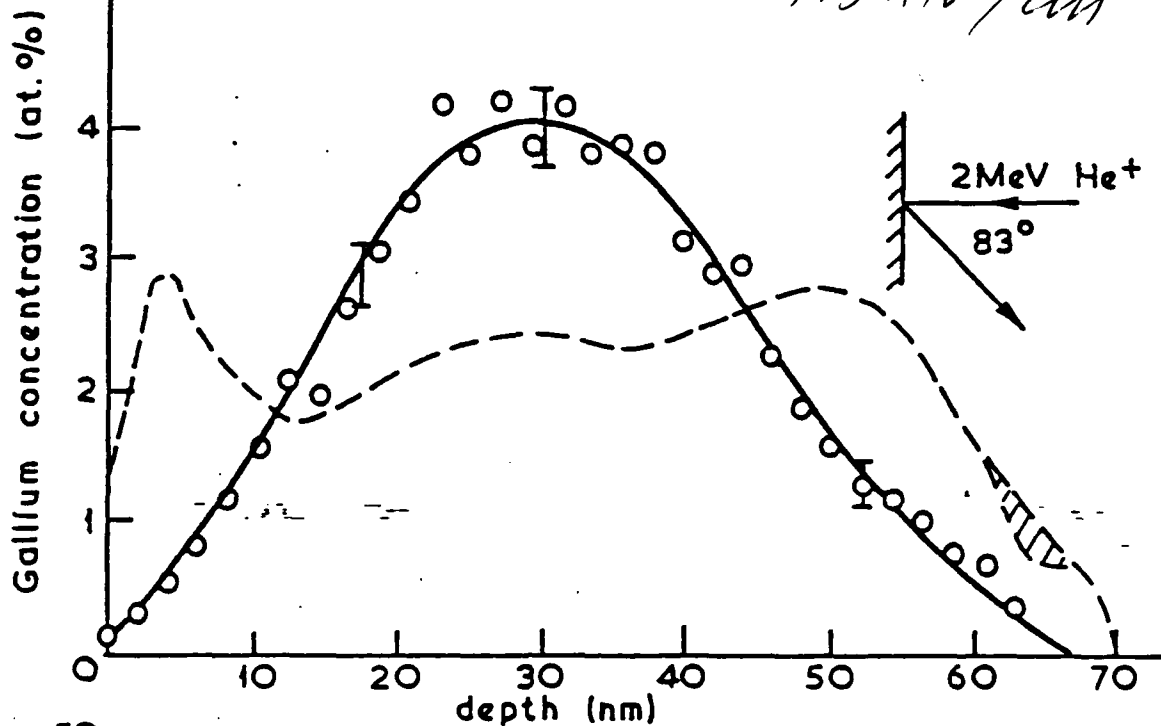


Fig. 1

Epitaxial regrowth of Gallium implanted Silicon,  
high Gallium concentrations.

$7.5 \times 10^{15} / \text{cm}^2$

(a)



(b)

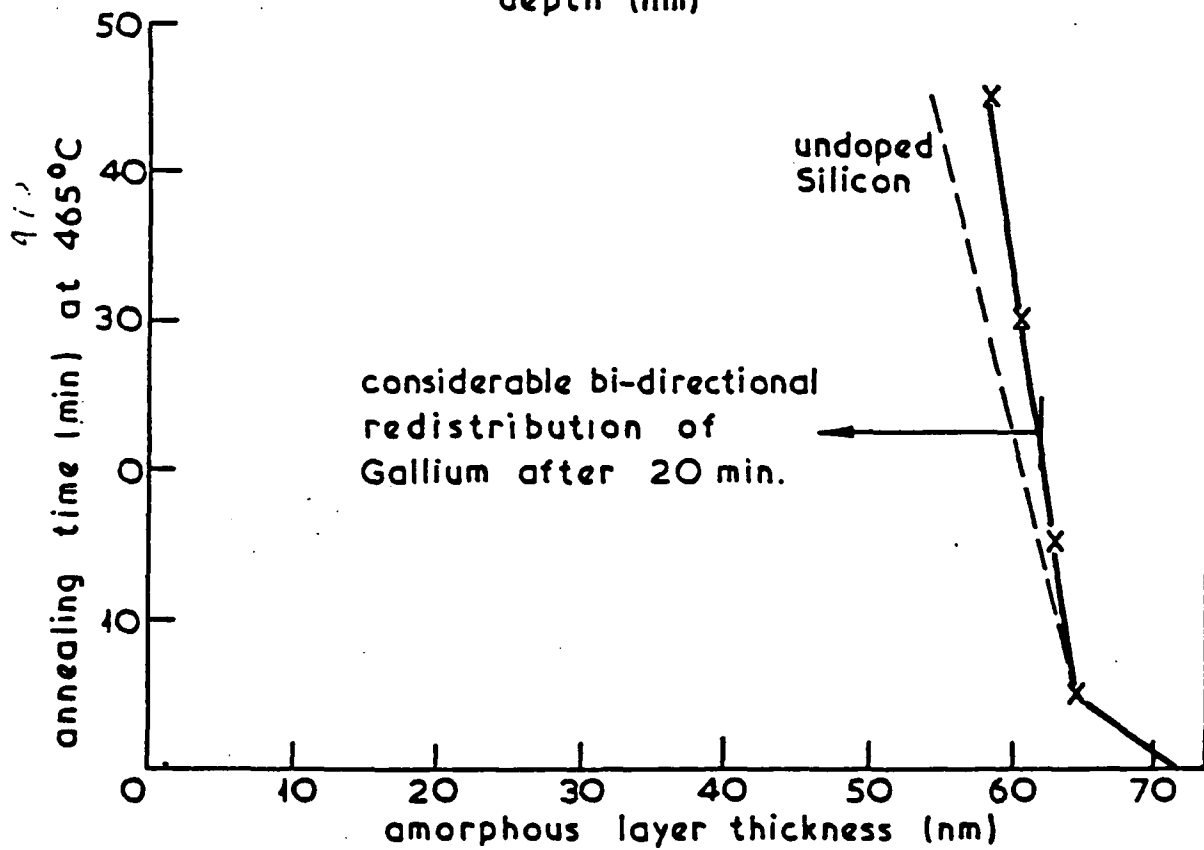
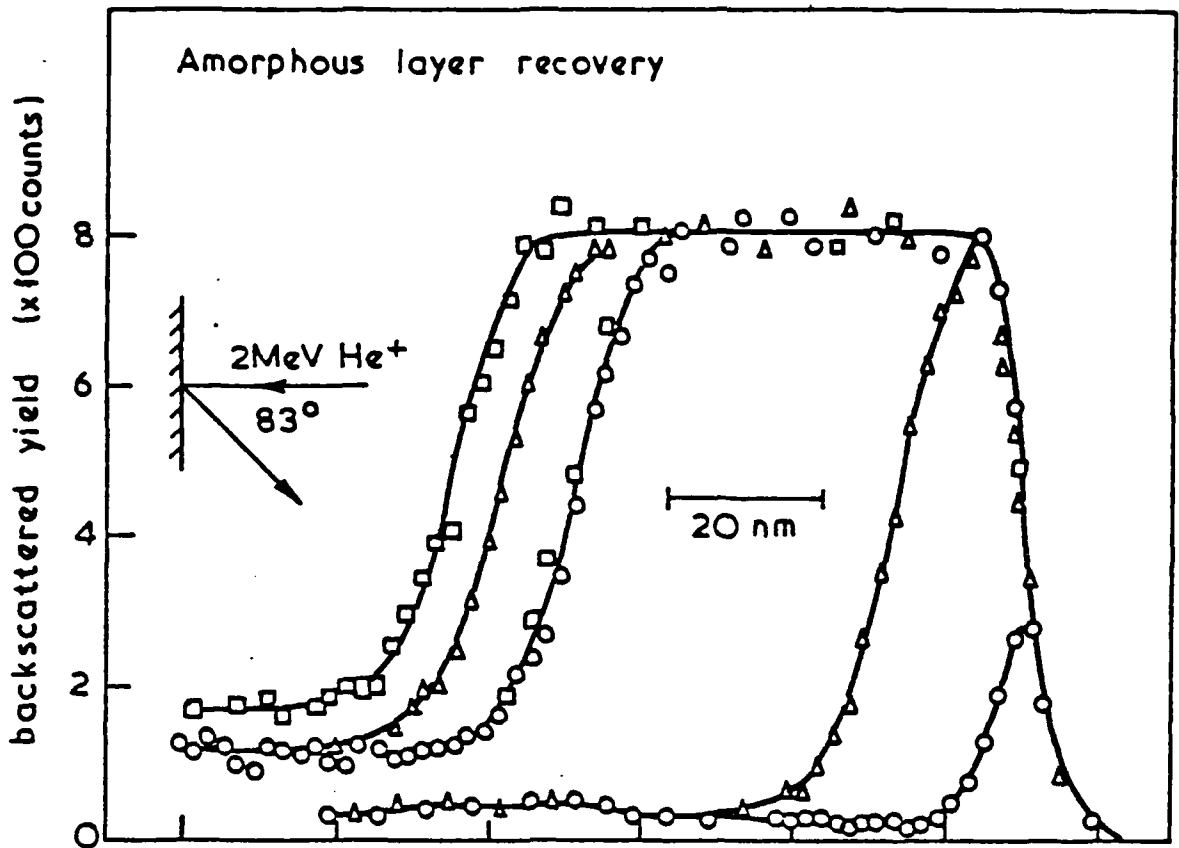


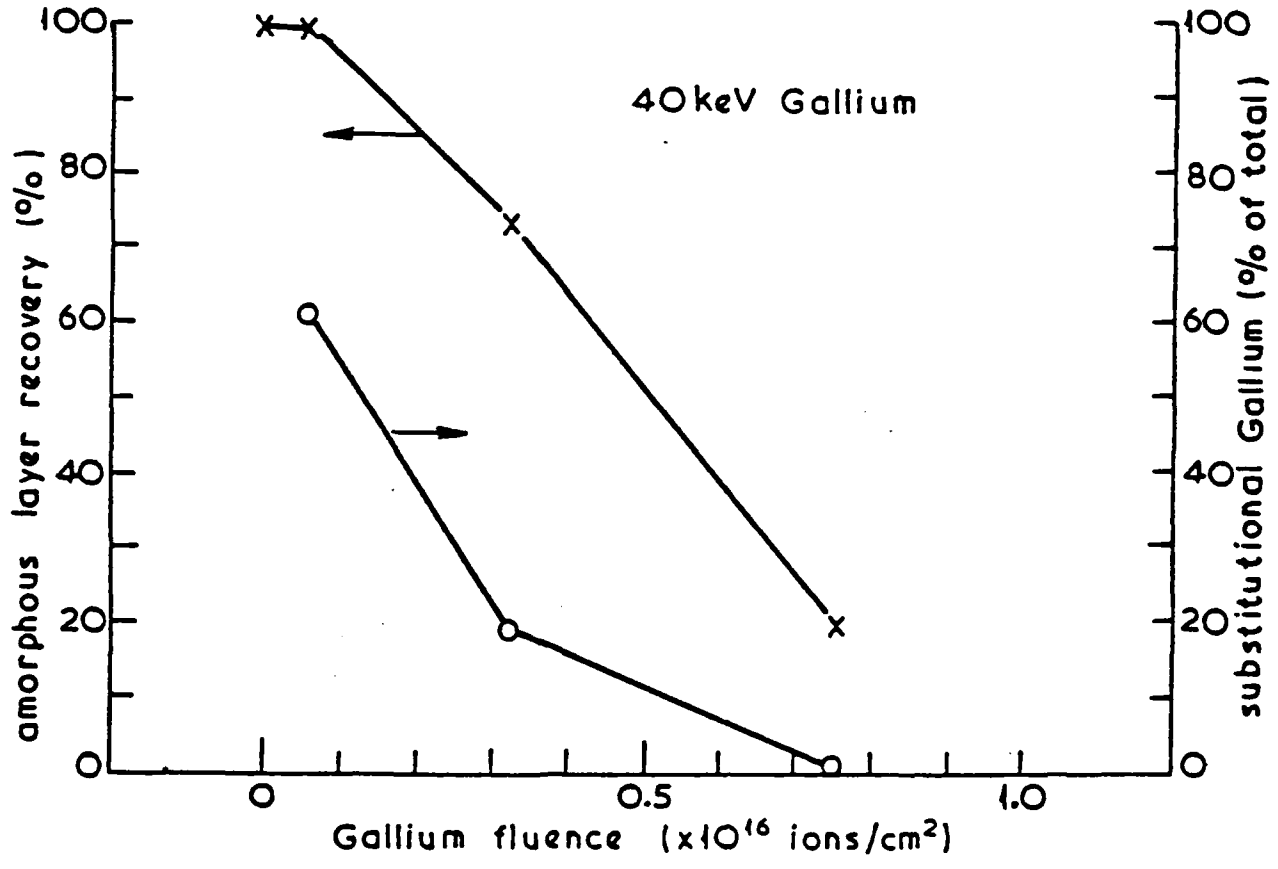
Fig. 2



(a)



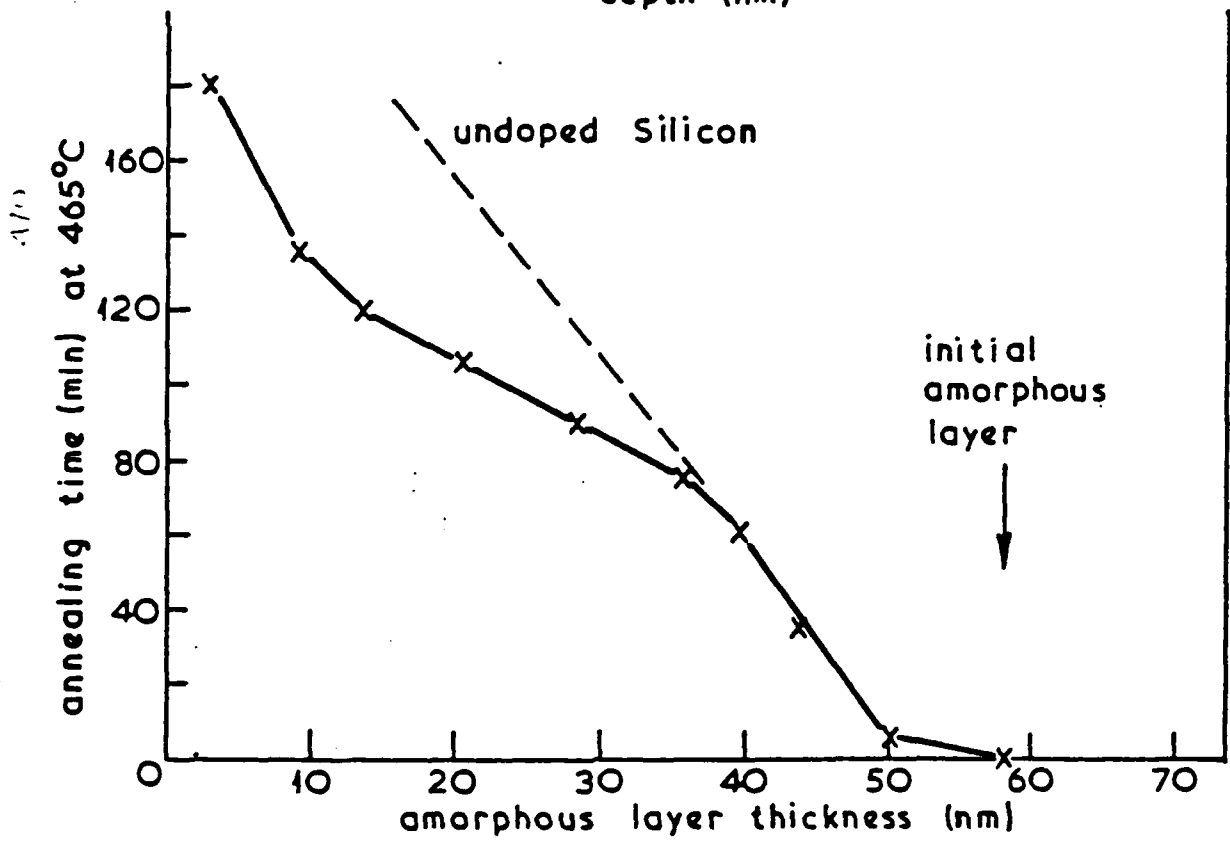
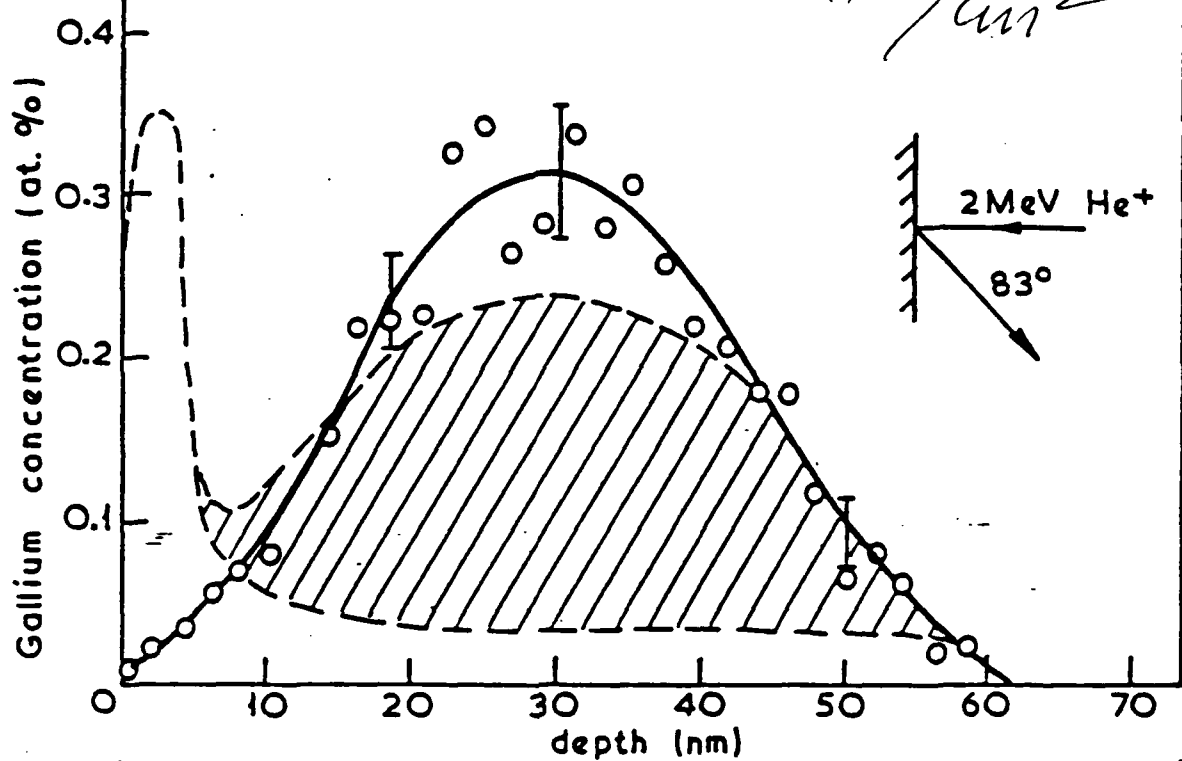
(b)



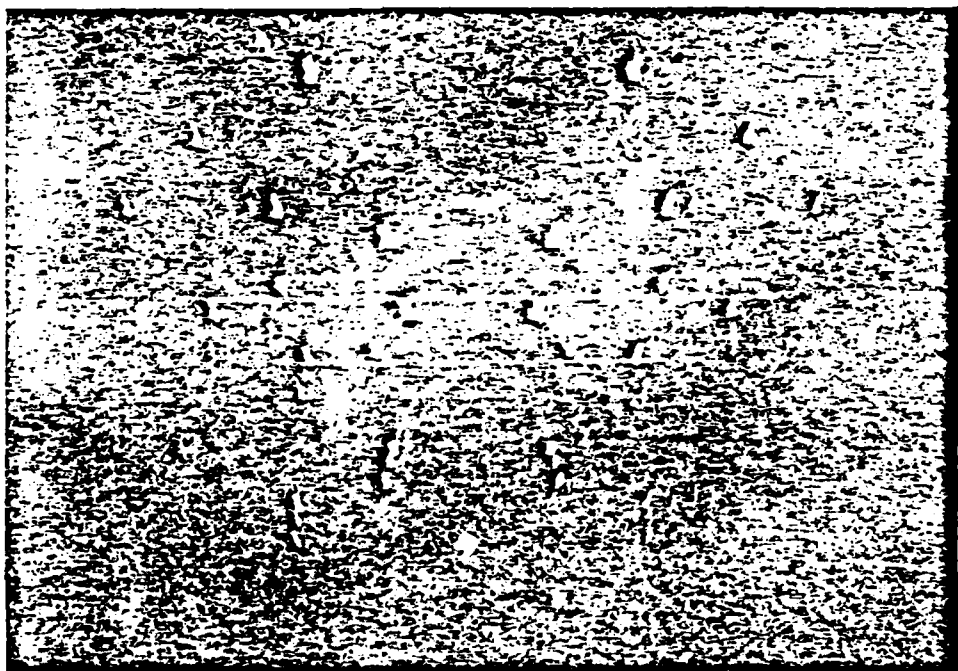
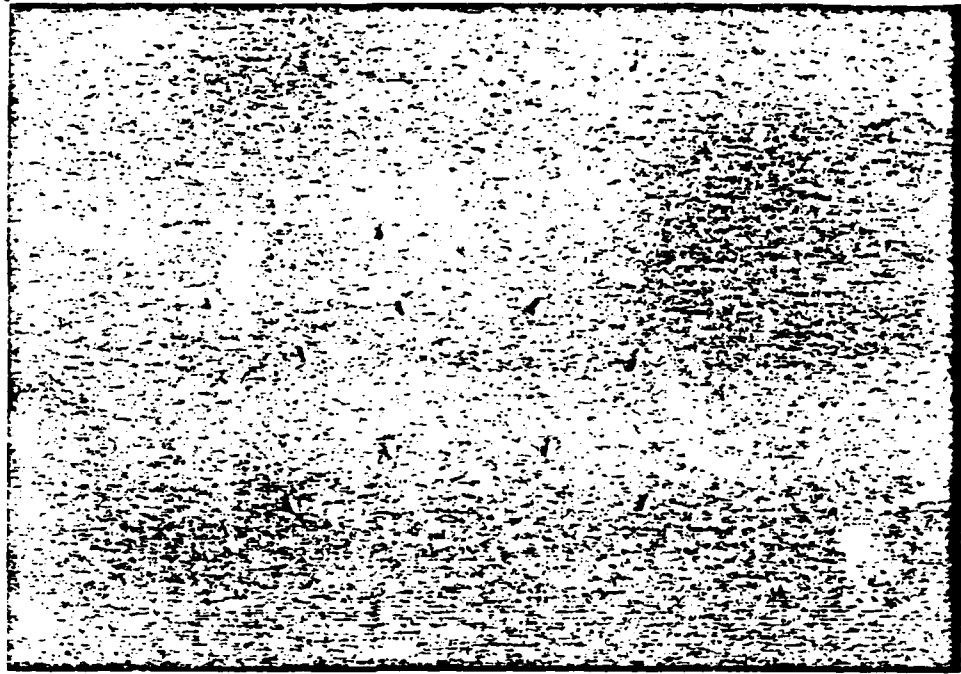
- 5.9. 4

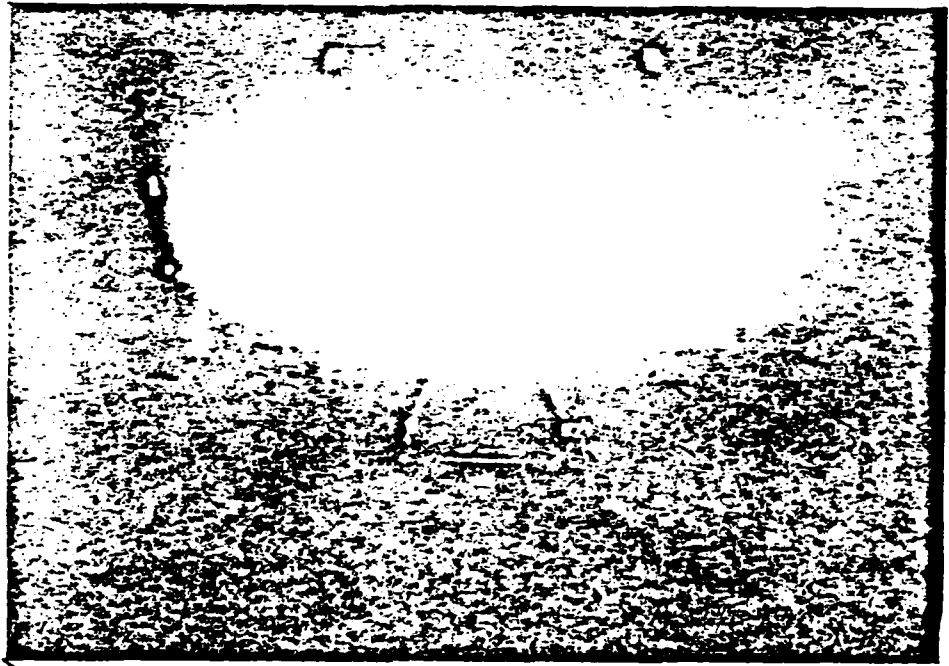
Epitaxial regrowth of Gallium implanted Silicon,  
 low Gallium concentration.

$6 \times 10^{14} / \text{cm}^2$



= Fig. 3





001 002 003 004 005 006 007 008 009 010 011 012 013 014 015 016 017 018 019 020 021 022 023 024 025 026 027 028 029 030 031 032 033 034 035 036 037 038 039 040 041 042 043 044 045 046 047 048 049 050 051 052 053 054 055 056 057 058 059 060 061 062 063 064 065 066 067 068 069 070 071 072 073 074 075 076 077 078 079 080 081 082 083 084 085 086 087 088 089 090 091 092 093 094 095 096 097 098 099 100

## ION IMPLANTATION DAMAGE IN InP

### ABSTRACT

The disorder generated by 40 keV light ( $N^+$ ) and heavy ( $Bi^+$ ) ion irradiation of InP at 40K and room temperature has been measured, using Rutherford backscattering channelling techniques, as a function of ion flux density and fluence. For the light ion irradiation the damage retained in the substrate is highly dependent upon irradiation temperature and upon flux density for room temperature irradiation. Such dependencies are much weaker for heavy ion irradiation. These results, together with the fluence dependence of disorder, are consistent with a mainly direct impact amorphisation, stable against annealing, process with heavy ion implantation and a mainly simpler defect generation, unstable against annealing, process with light ion implantation.

Studies of disorder generation in both the In and P sublattices are also discussed.

---

\*Institute of Low Energy Nuclear Physics, Beijing Normal University, Beijing, China.

## INTRODUCTION

The use of compound semiconductors in the electronics industry has grown considerably in the last few years, due, mainly, to the wide variety of electronic and electro-optical properties exhibited by these materials. Doping these compounds by conventional diffusion techniques is, however, quite difficult since many of the useful substrates have rather low melting points and the solubility of potentially promising dopants is often very low. Ion implantation is, therefore, a very attractive alternative for doping compound semiconductors and, indeed, it has already been extensively used for such applications<sup>(1)</sup>.

Indium phosphide and its ternary and quaternary compounds are currently receiving attention for electro-optical and electronic applications, and ion implantation is commonly employed as a doping technique for these materials. As with other semiconductor materials, both elemental and compound, ion implantation of InP can result in severe radiation damage. This damage is normally detrimental for doping applications, but it is extremely useful to know the form of the disorder (i.e. point defects, extended defects or amorphous layer), as this will determine the optimum annealing procedure for damage removal<sup>(2)</sup>. In addition, there are applications where radiation damage is a desirable result of implantation<sup>(1)</sup>, (e.g. for providing electrically isolated regions by compensating carriers), and again it is desirable to know the form and distribution of the disorder.

Despite the relatively recent interest in InP, considerable experimental data exists for implantation into this material<sup>(1-6)</sup>. Only recently, however, have somewhat exploratory measurements of damage profiles and their fluence dependence been reported<sup>(4-6)</sup>. In such investigations only the sum of the In and P displacements have been observed. In the present study we report on the fluence and flux dependence of disorder in InP for two cases

where quite different damaging mechanisms may be expected to operate, i.e. low and high mass ions. Investigations were carried out at both room temperature and 40K and the separate depth distributions and total displaced atom densities of In and P were observed.

### EXPERIMENTAL

Commercially prepared (100) InP samples were bombarded with 40 keV  $N^+$  and  $Bi^+$  ions at room temperature, to doses up to  $5 \times 10^{16}$  ions/cm<sup>2</sup>. A variety of current densities between  $1 \mu a \text{ cm}^{-2}$  and  $10 \mu a \text{ cm}^{-2}$  were employed for implantation so that dynamic annealing processes could be investigated. The target chamber pressure was maintained at  $\sim 10^{-7}$  torr during implantation and samples were tilted  $\sim 7^\circ$  from normal incidence to minimise ion channelling effects. After implantation samples were analysed by Rutherford backscattering and channelling of 2 MeV  $He^+$  ions on a separate accelerator at Salford. The ion current densities indicated above are average values for the swept line focus ion beam. Instantaneous current densities are up to a factor of  $10^2$  larger than these values.

In compatible experiments conducted at McMaster University 40 keV  $N^+$  and  $Bi^+$  were implanted into InP at 40K, at much lower current densities. These implanted samples were then analysed, in situ, with MeV  $He^+$  ion backscattering/channelling, with the analysis beam derived from a separate on-line accelerator. This facility has been described elsewhere<sup>(7)</sup>.

Backscattering/channelling spectra were recorded following each implant and random and aligned (100) axis data acquired for each implant condition. It was clearly observed that the analysing  $He^+$  probe beam caused substantial disorder production in the InP, even at room temperature. Si shows a similar

behaviour at low temperatures<sup>(8)</sup>. Consequently the disorder-He<sup>+</sup> fluence behaviour was determined for a non heavy ion implanted InP substrate over a fluence range much larger than, but including, the low fluence He<sup>+</sup> probe level employed for heavy ion induced disorder analysis. In this way disorder introduced during analysis could be subtracted (linearly<sup>(8)</sup>) from the observed disorder data. In order to convert measured backscattering data to displaced atom densities and to fit a depth scale to the backscattered energy scale, standard routines of energy variable scattering cross-section, linear dechannelling approximation and stopping powers (deduced from tables) were employed.

## RESULTS AND DISCUSSION

Figure 1 displays typical RBS/channelling data following increasing fluence 40 keV N<sup>+</sup> implantation at room temperature and for a N<sup>+</sup> flux density equivalent to 1  $\mu\text{a cm}^{-2}$ . The results displayed are in fact smoothed with respect to the raw data by five point averaging. Even with this procedure, it is clear that retrieval of displaced atom densities as a function of depth (from the increased backscattering/channelled yield as a function of channel number or backscatter energy) for P atoms, in particular, is difficult because of the high dechannelling continuum in the P region of the backscattering spectrum. For this reason, we have not attempted here to derive accurate displaced atom densities for comparison between the P and In depth distributions. Total, depth integrated, disorder densities have been derived from data such as in Figure 1 however, with an estimated error in this density,  $N_d$ , for P of  $\pm 10\%$ . The results of such evaluations are shown in Figure 2a where  $\log N_d$ , for P and In is plotted as a function of  $\log$  (fluence,  $\phi$ ) for a 1  $\mu\text{a cm}^{-2}$  ion flux. In deducing these curves subtractions



of the disorder produced by the 2 MeV analysing  $\text{He}^+$  beam<sup>(8)</sup>, which was observed to be substantial even at room temperature, from the apparent measured  $\text{N}^+$  induced disorder were effected. Within the accuracy of the measurements Figure 2a suggests that P and In displaced atom densities are approximately equal. The less reliable depth distribution data also suggest identity of the P and In displaced atom densities at all depths.

Disorder-fluence data similar to that of Figure 2a was obtained at different ion flux densities of  $1 \mu\text{a}$ ,  $5 \mu\text{a}$  and  $10 \mu\text{a cm}^{-2}$  with results displayed in Figure 2b for the more accurately determined In displacements. It is clear that except at the highest disorder levels, near quasi-saturation where disorder increases only slowly with fluence, the effect of increasing ion flux density is to increase the disorder. The effect is equally pronounced in the depth distributions of displaced atom density which are shown in Figures 3a and 3b for In displacements for  $\text{N}^+$  fluences of  $5 \times 10^{14} \text{ m}^{-2}$  and  $10^{16} \text{ cm}^{-2}$  respectively for ion flux densities of  $1 \mu\text{a}$ ,  $5 \mu\text{a}$  and  $10 \mu\text{a cm}^{-2}$  for each fluence. These results clearly indicate that increasing ion flux density leads to some increase in disorder at all depths and that the enhancement becomes more pronounced at lower disorder levels, i.e. the effect is more pronounced at all depths for the lower fluence data of Figure 3a and more pronounced deeper in the solid in both Figures 3a and 3b.

Similar results to the above were obtained using the heavier Bi ions at 40 keV. Since disorder is concentrated nearer the surface the P displaced atom density is even more difficult to deduce and so results only for In will be given. Figure 4 displays  $\log N_d / \log \phi$  data for 40 keV implants at room temperature, at low fluence levels, with an  $0.01 \mu\text{a cm}^{-2}$  flux density, but at higher fluence levels at  $1 \mu\text{a cm}^{-2}$ . This strategy was required to obtain accurate fluence values (longer implant times) at the lower fluence levels which are demanded because of the very rapid initial disordering rate (compare the high disorder level achieved with low fluence  $\text{Bi}^+$  implants

of Figure 4 with the much lower disorder levels for corresponding fluences of  $N^+$  in Figure 2a) but also to allow acceptable implant times at higher fluence levels. Figure 4 also shows data obtained with 40 keV  $Bi^+$  implants at 40 K using an on-line implanter -  $He^+$  accelerator analysis system at McMaster University and described elsewhere<sup>(7,8)</sup>. This figure indicates that at high fluence, and near quasi-saturation disorder, the total disorder is rather independent of substrate temperature and it was also observed that at high fluence (disorder) levels, the disorder was almost flux density independent. This behaviour is illustrated in Figure 5b which shows the (approximate) depth distribution of In displaced atoms for an implant fluence, at room temperature, of  $5 \times 10^{14} \text{ cm}^{-2}$  and for flux densities of  $1 \mu\text{a}$ ,  $5 \mu\text{a}$  and  $10 \mu\text{a cm}^{-2}$ . Although there is an increase in disorder in the deeper regions of the crystal with increasing flux density the effect is small but at lower fluence and disorder levels the effect is larger but less marked than for  $N^+$  implants. Figure 5a illustrates this comparatively larger increase in disorder at all depths with increasing flux density for a fluence of  $10^{14} \text{ Bi}^+ \text{ cm}^{-2}$ .

In comparing and discussing the preceding data we note first that the initial rate of disorder production (from the low fluence, displaced atom intercept) is much greater for  $Bi^+$  ions at both room temperature and low temperature than for  $N^+$  ions. This behaviour is entirely consistent with earlier observations with Si<sup>(8,9)</sup> and GaAs<sup>(10)</sup> substrates and is a reflection of the high energy density deposition conditions induced by the heavier ion which leads to displaced atom densities much in excess of linear cascade predictions and is the result of largely direct impact amorphisation processes<sup>(11)</sup>. The initial linear slope of the  $\log N_d / \log \phi$  plot for low temperature implants is a further reflection of the probable dominance of direct amorphisation in individual cascades or spikes<sup>(8,9,10,11)</sup>. If the present 40 keV  $Bi^+$ , low-temperature data is compared with similar measurements

for GaAs substrates<sup>(10)</sup> (similar mean mass target) it is found that the disorder at all fluence levels including quasi-saturation, is approximately equal. It is easy to understand the reason for this similarity since cascade volumes and energy densities would be expected to be similar for the two substrates whilst damage depth profiles, which dictate amorphous layer thicknesses<sup>(8,10)</sup> would be expected to be similar also.

The much lower disorder production rate for  $N^+$  implantation suggests, as for Si<sup>(8,9)</sup> and GaAs<sup>(10)</sup> substrates, that the major disordering process is one of simpler defect production with increasing defect accumulation until local collapse to amorphousness occurs at a critical defect density<sup>(12)</sup>. As these amorphous zones accumulate and overlap a continuous amorphous layer results as indicated by the backscattering data of Figure 1. The lower displaced atom density at the quasi-saturation level for  $Bi^+$  implants as compared to  $N^+$  implants is a direct reflection of the shallower implant range and disorder production depth for the heavier ion which leads to thinner amorphous layer production.

It is also important to note that, to the limit of present accuracy, there are no major differences (for  $N^+$  implantation) of either the depth distributions at total displaced atom densities of the In & P components. We did not observe, therefore, the theoretically predicted<sup>(13)</sup>, non-stoichiometric spatial distributions of In & P vacancies and interstitials. It should be remembered that these predictions indicate only small non-stoichiometries, within the error limits of the present data particularly for P, whilst the predictions refer to different implant conditions (more energetic ions than employed here).

Turning next to the effects of variation of ion flux density it is immediately apparent that for both implant species and all fluence conditions, the disorder increases with-increasing flux density. The variation of disorder

with flux density is quite generally an indication<sup>(14)</sup> of the operation of defect migration and annealing processes which compete with the generation process. Thermal annealing rates are expected to increase with increasing substrate temperature and reduce disorder levels and consequently the increase in disorder with increasing flux density is a clear indication that the increasing flux density (and thus beam power dissipated in the substrate) does not result in sufficient temperature increase to accelerate annealing. The process is thus one where the increasing flux density more successfully competes with thermal (flux density independent) annealing to produce more stable disorder<sup>(15)</sup>.

It is notable that the effect of increasing flux density is most marked for the lighter ion implant, at the lower fluence and disorder levels for both ion species and in the deeper components of the disorder-depth distributions. In all these conditions the nature of the disorder is expected to be of simpler defect form, even in the case of the heavy ion irradiation where, in the deep tails of individual collision cascades the energy deposition density will be insufficient to generate spike conditions and at the radial peripheries of such individual cascades nearer the surface the damage will be simpler before complete amorphous layers have accumulated.

It is thus reasonable to conclude that the flux density influence on measured disorder production is a clear indication of the production and subsequent migration, at room temperature, of simple defects. In earlier studies of disorder production in InP, under mainly low energy deposition density conditions, there are also signs of annealing processes, both from the post-irradiation long term annealing at room temperature studies<sup>(4)</sup> and the rapid increase with temperature<sup>(2,3,5)</sup> near room temperature of the fluence required for layer amorphisation. Annealing clearly occurs under all irradiation conditions employed here, to a greater or less extent, but is most important for lighter projectiles. There is again a clear indication of the influence

of simpler defect production mechanisms for lower energy deposition density (and associated local defect density) conditions and direct impact amorphisation (or some similar form of thermally stable disorder) for higher energy deposition density conditions. The existence of some annealable disorder, even with the heavy ion (higher energy density deposition) is not only evident in the dependence of disorder on flux density shown in Figure 5 but also in the increase in the low fluence disorder with decreasing substrate temperature shown in Figure 4. Similar low temperature studies for  $N^+$  implants are currently in progress and will be reported elsewhere and, in view of the very significant influence of flux density for this ion species, are expected to reveal very large increases in disorder generation rate when compared to the room temperature data of Figure 2.

In view of the observed flux density effects and the implied existence of annealing processes it is clear that measurements of disorder generation rates per ion ( $N_d^*$ ) should only be attempted with low temperature substrates, as reported for Si (8,9) and GaAs (10) in order to compare with model (e.g. linear cascade or spike) predictions. It is for this reason that detailed quantitative evaluations of  $N_d^*$  have not been attempted here but only qualitative comparisons between  $Bi^+$  and  $N^+$  implants.

### CONCLUSION

This study has revealed that probable disordering mechanisms resulting from both light and heavy, relatively low energy, ion impact on InP are similar to and fit into the general scheme proposed for both Si (8) and GaAs (10). Thus implantation resulting in high energy deposition density conditions leads predominantly to direct impact amorphisation processes whereas lower energy deposition density conditions lead to simpler defect production which

accumulates and transforms to amorphousness at critical levels. These hypotheses are supported by the strong influence of ion flux density upon stable disorder production for lighter ion implantation and the weaker but evidently similar effects with heavy ion implantation, and in this latter case the influence of substrate temperature.

It is clear that in technological applications careful control of ion flux density and substrate temperature should be exercised and that if amorphous layer structures are desirable high flux, low temperature conditions are advised but if such structures are undesirable low flux, elevated temperature conditions are advised.

Within the limits of experimental accuracy, no major differences in the stoichiometry of In and P displacements were observed.

#### ACKNOWLEDGEMENTS

We are grateful to Dr D A Thompson and his colleagues at McMaster University for assisting in the low temperature studies and to NATO for a research grant which aided the collaborative part of this work.

REFERENCES

- (1) D V Morgan, F H Eisen and A Ezis. IEE Proc 128 109 (1981).
- (2) D E Davies. J Crystal Growth 54 150 (1981).
- (3) W Rothemund and C R Fritzsche. J Vac Sci Technol 16 968 (1979).
- (4) E F Kennedy. Appl Phys Letters 38 375 (1981).
- (5) T Inada, S-i Taka and Y Yamamoto. J Appl Phys 52 4863 (1981).
- (6) S S Gill, B J Sealy and K G Stephens. J Phys D Appl Phys 14 1915 (1981).
- (7) R S Walker and D A Thompson. Nucl Instrum & Meth 135 389 (1976).
- (8) D A Thompson, A Golanski, H K Haugen, D V Stevanovic, G Carter and C E Christodoulides. Rad Effects 52 69 (1980).
- (9) D A Thompson and R S Walker. Rad Effects 36 91 (1979).
- (10) N P Tognetti, G Carter, D V Stevanovic and D A Thompson. Rad Effects. To be published.
- (11) M L Swanson, J R Parsons and C W Hoelke. Radiation Effects in Semiconductors. 1971 (Eds. J W Corbett and G D Watkins, Gordon & Breach Ltd, New York) p359.
- (12) J F Gibbons. Proc IEE 60 1062 (1972).
- (13) L A Christel and J F Gibbons. J Appl Phys 52 5050 (1981).
- (14) G Carter and W A Grant. Ion Implantation of Semiconductors (Edward Arnold, London) 1976.
- (15) G Carter and R G Elliman. Rad Effects Letters. To be published (1982).

## FIGURE CAPTIONS

- Fig. 1 Random and aligned RBS spectra of 2 MeV  $\text{He}^+$  ions from 40 keV  $\text{N}^+$  implanted InP at room temperature for different incident  $\text{N}^+$  fluences.
- Fig. 2a The number of displaced In & P atoms ( $N_d$ ) in InP as a function of 40 keV  $\text{N}^+$  ion implantation fluence at room temperature. The ion current density was equivalent to  $1 \mu\text{a cm}^{-2}$ .
- Fig. 2b The number of displaced In atoms in InP as a function of 40 keV  $\text{N}^+$  ion implantation fluence at room temperature. Ion current densities equivalent to 1, 5 and  $10 \mu\text{a cm}^{-2}$  were employed.
- Fig. 3a The effective depth (channel no.) distribution of displaced In atoms in InP following 40 keV  $\text{N}^+$  ion implantation at room temperature to a constant fluence of  $5 \times 10^{14}$  ions  $\text{cm}^{-2}$  at equivalent flux densities of 1, 5 and  $10 \mu\text{a cm}^{-2}$ .
- Fig. 3b The effective depth (channel no.) distribution of displaced In atoms in InP following 40 keV  $\text{N}^+$  ion implantation at room temperature to a constant fluence of  $10^{16}$  ions  $\text{cm}^{-2}$  at equivalent flux densities of 1, 5 and  $10 \mu\text{a cm}^{-2}$ .
- Fig. 4 The number of displaced In atoms in InP as a function of 40 keV  $\text{Bi}^+$  ion implantation fluence at room temperature and at 40 K.
- Fig. 5a The effective depth (channel no.) distribution of displaced In atoms in InP following 40 keV  $\text{Bi}^+$  ion implantation at room temperature to a constant fluence of  $10^{14}$  ions  $\text{cm}^{-2}$  at equivalent flux densities of 1, 5 and  $10 \mu\text{a cm}^{-2}$ .



Fig. 5b

The effective depth (channel no.) distribution of displaced In atoms in InP following 40 keV Bi<sup>+</sup> ion implantation at room temperature to a constant fluence of  $5 \times 10^{14}$  ions cm<sup>-2</sup> at equivalent flux densities of 1, 5 and 10  $\mu$ a cm<sup>-2</sup>.

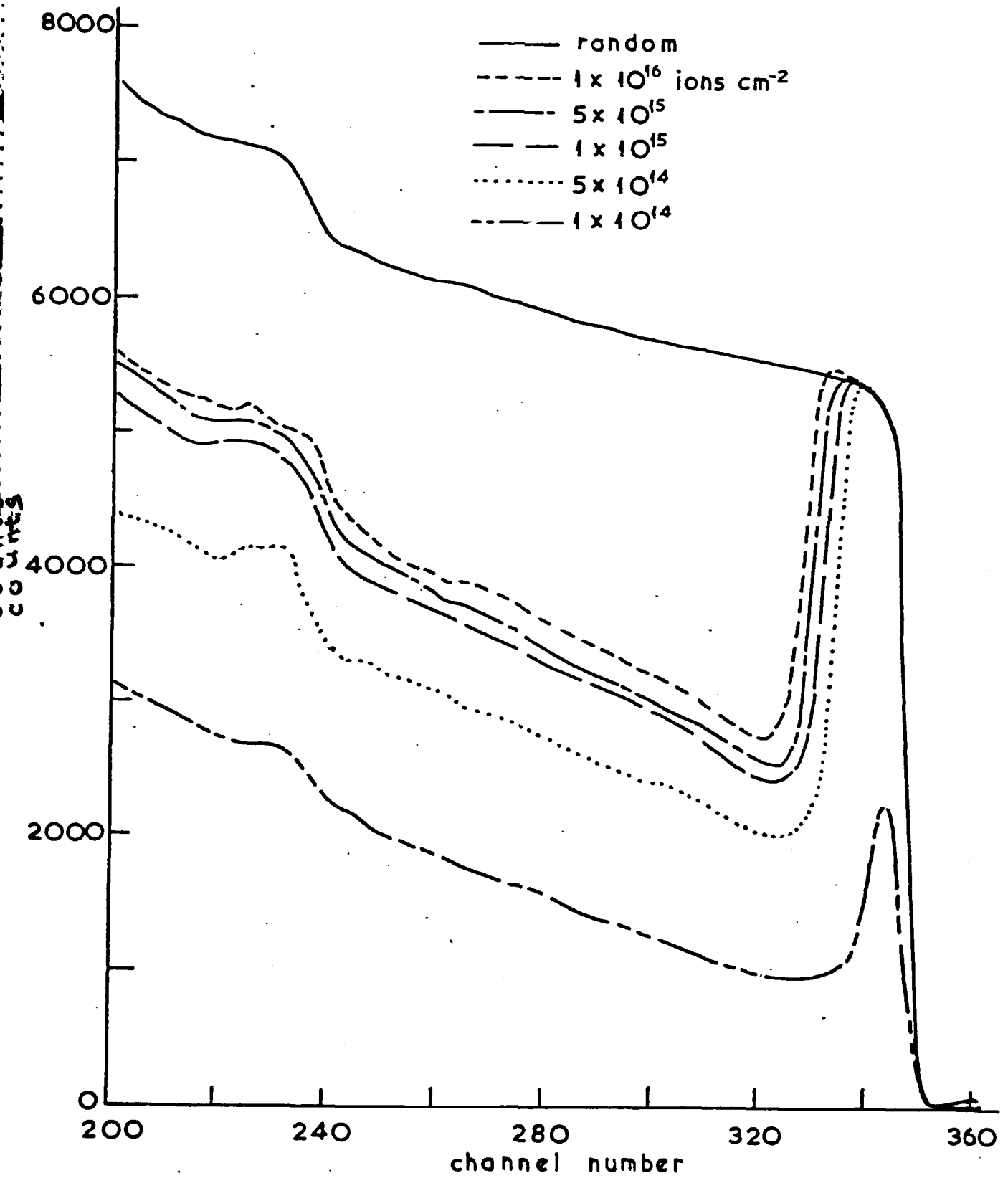


Fig 1

Number of displaced atoms  $\cdot \text{cm}^{-2}$

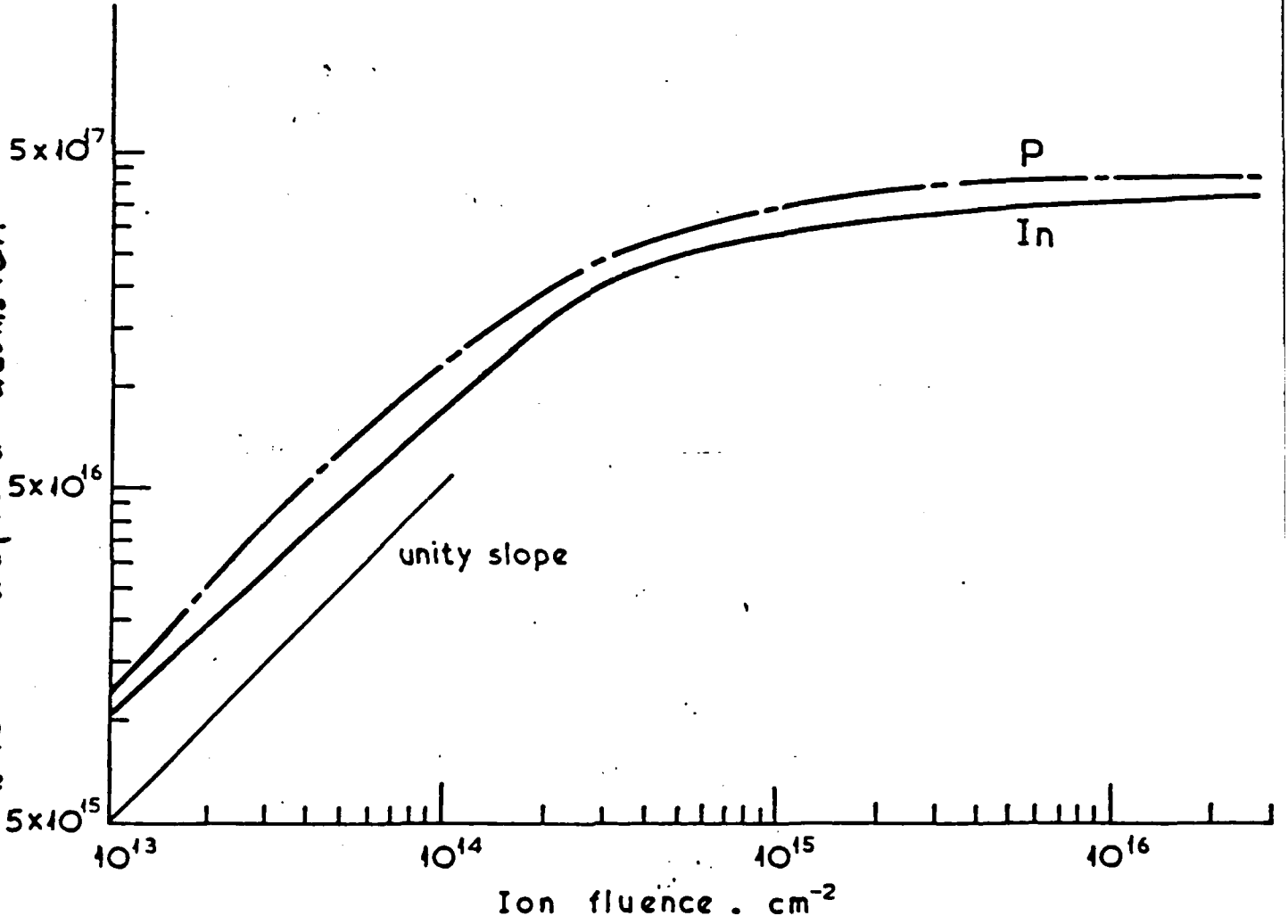


Fig 2a

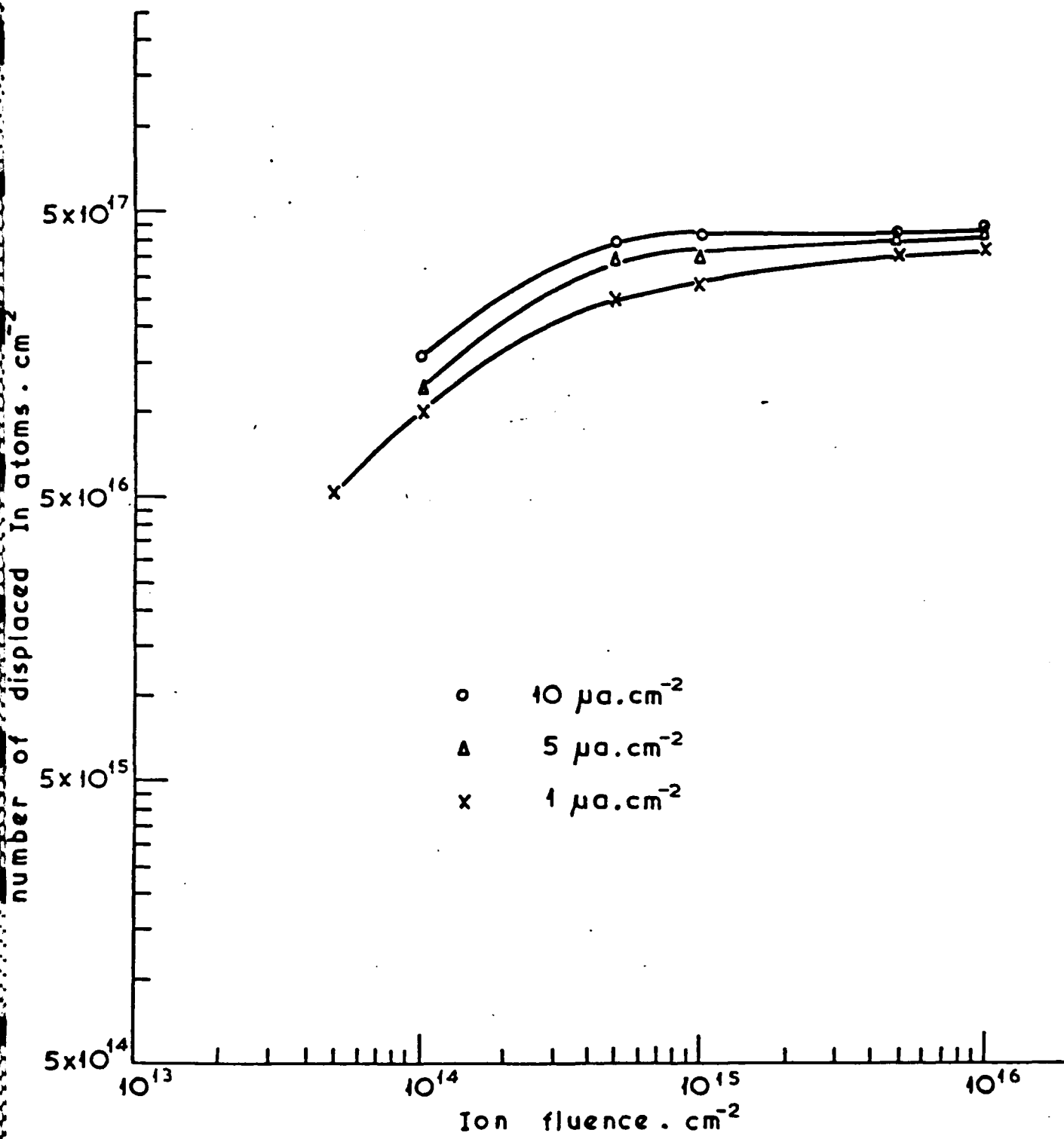


Fig 2b

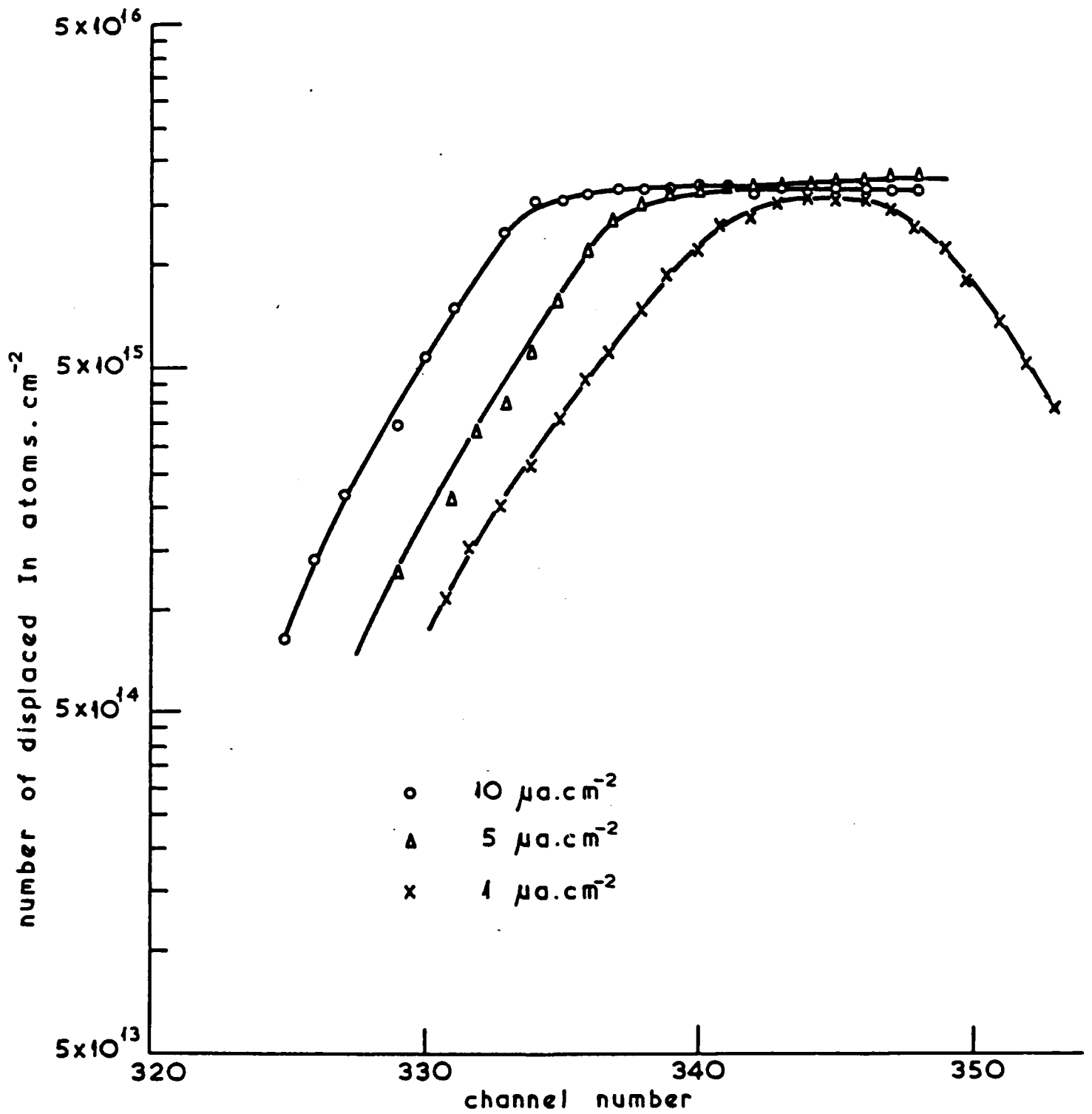
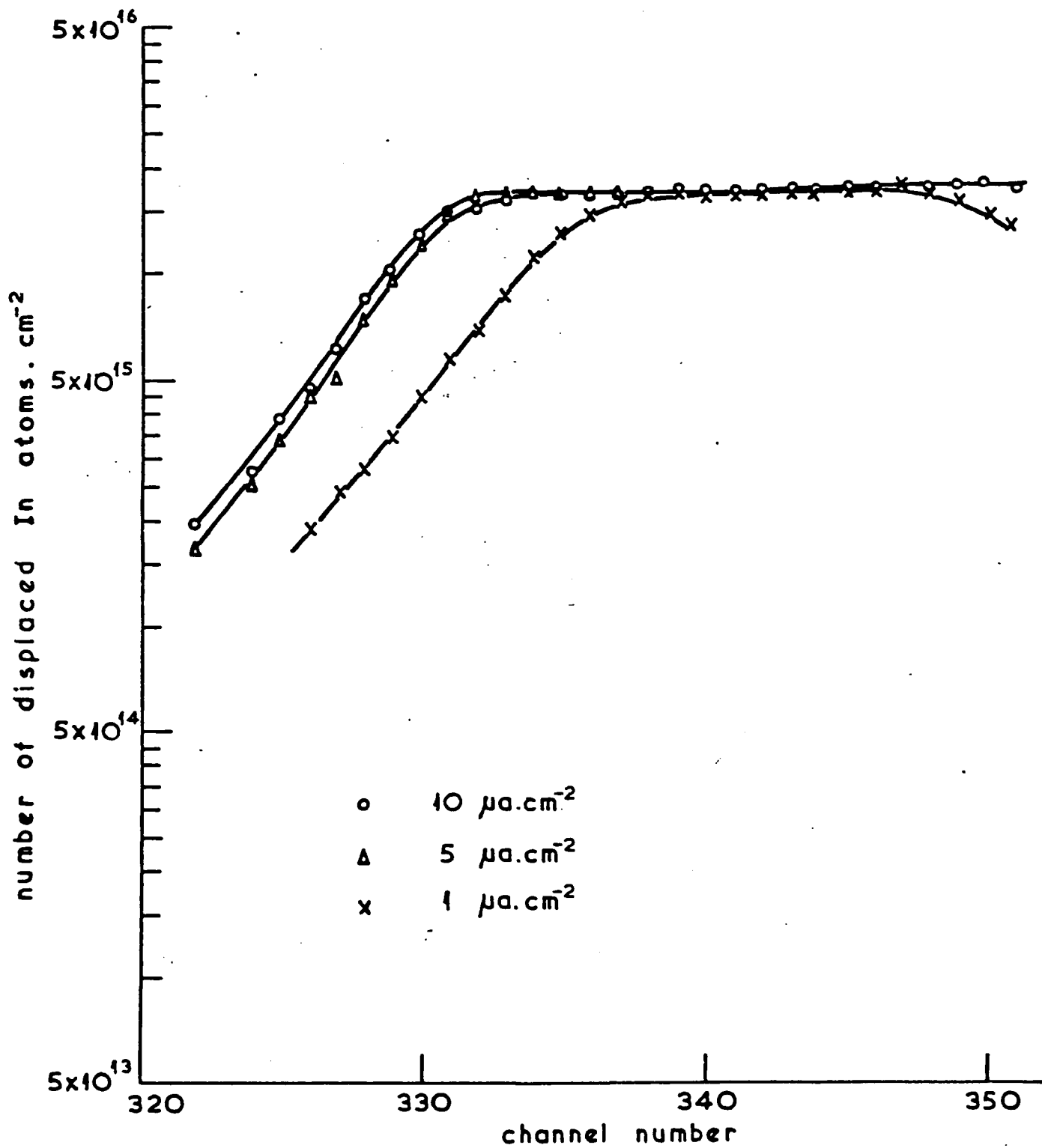


Fig 3 a



E u 3 b

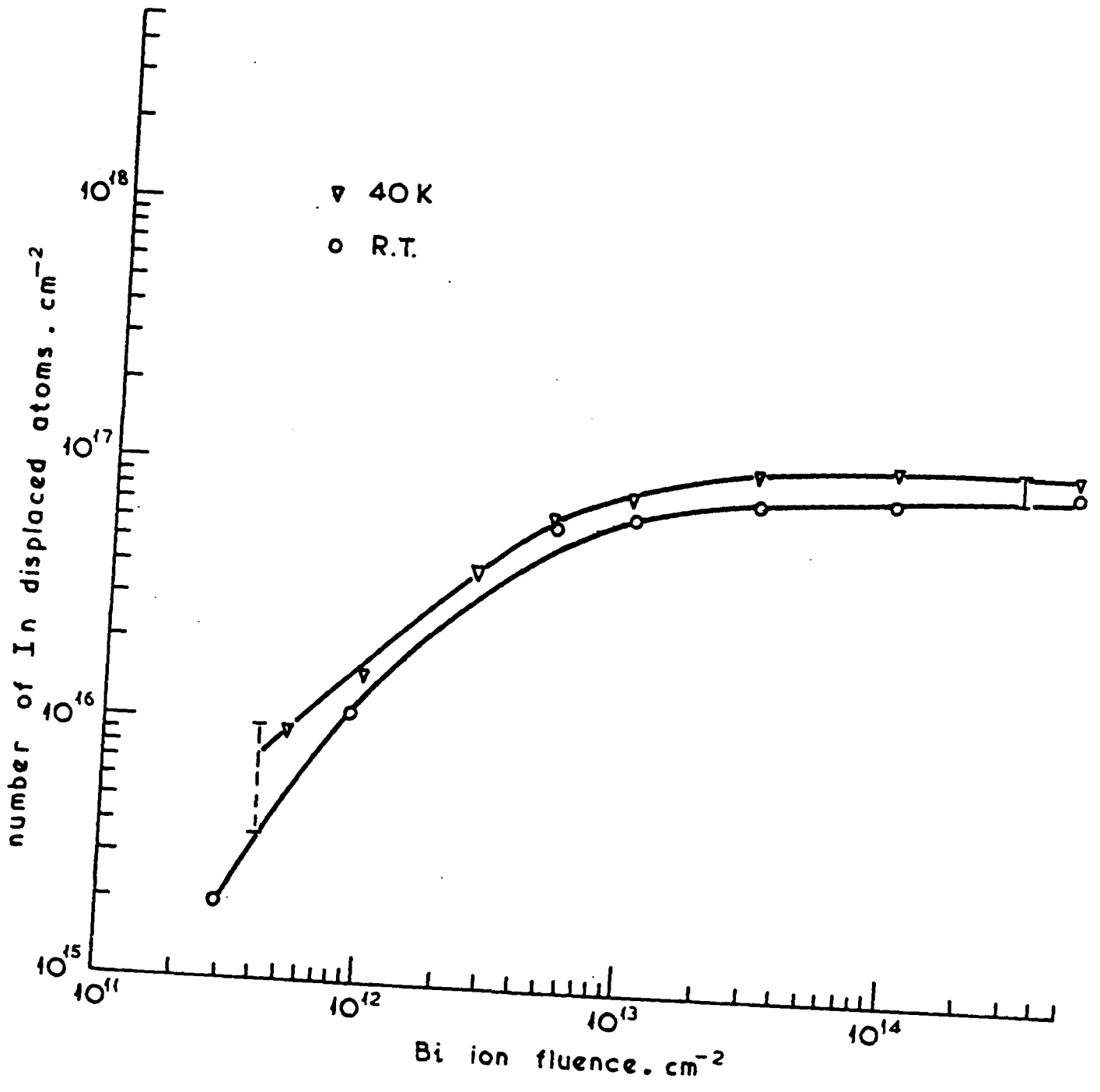


Fig. 4

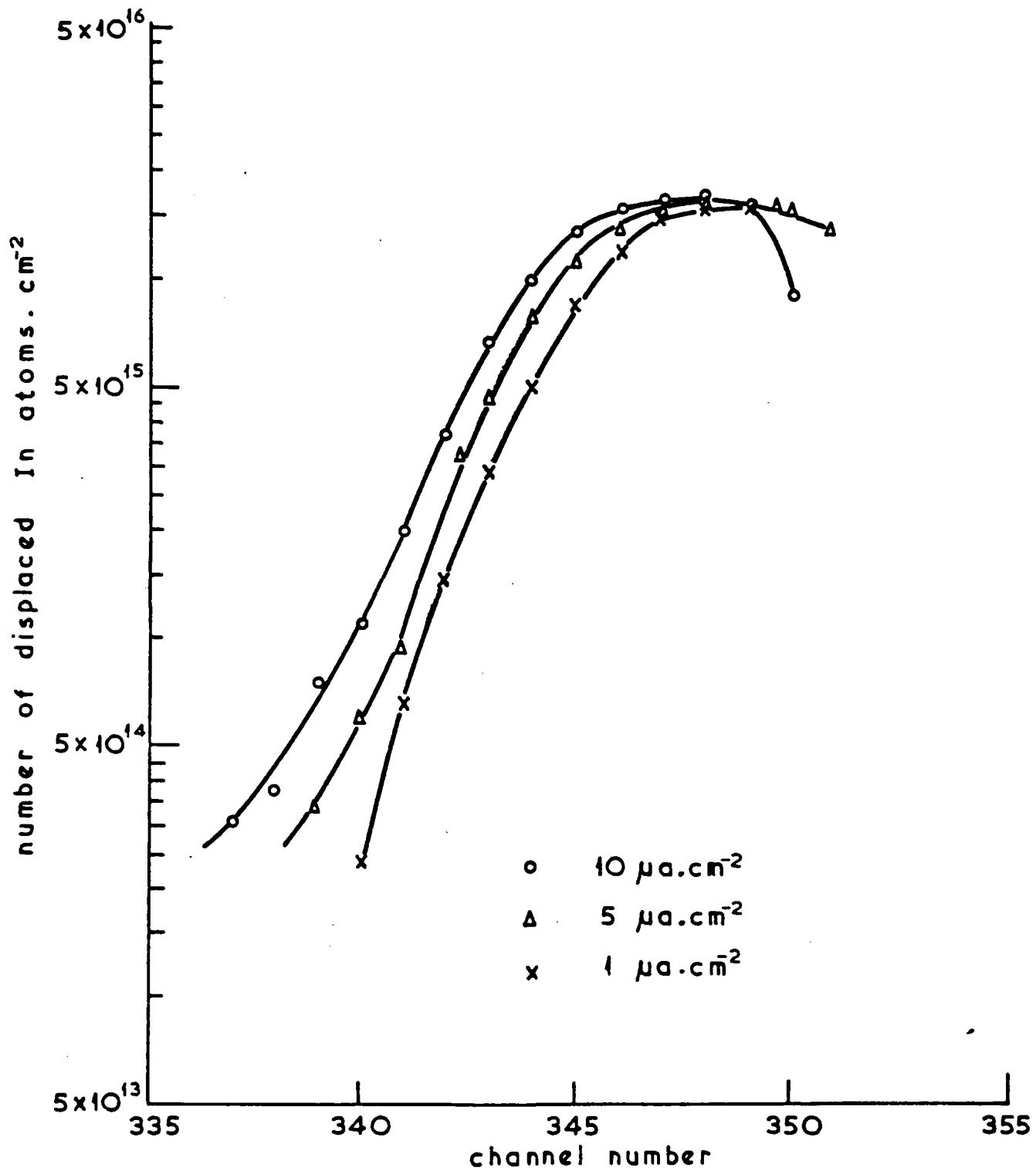


Fig 5a



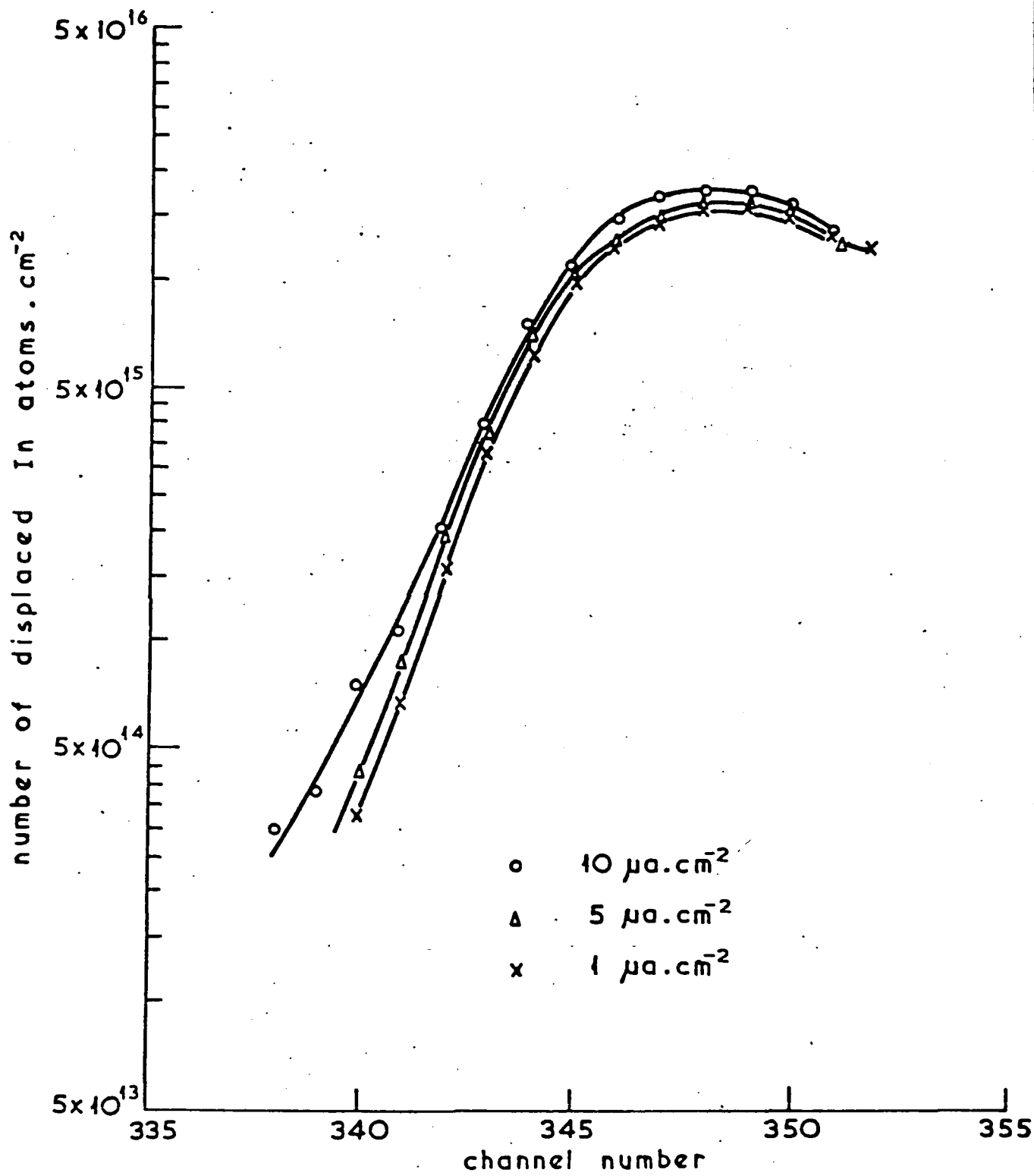


Fig 5b

DISORDER PRODUCTION AND ANNEALING DURING He ION RBS/CHANNELLING ANALYSIS  
OF InP

ABSTRACT

Studies of the interaction of 2 MeV He<sup>+</sup> ions, employed for Rutherford backscattering/channelling of disorder in InP, with the disorder generated by pre-implantation of 40 keV N<sup>+</sup> ions at room temperature are reported. It is shown that for initially undamaged substrates, He<sup>+</sup> irradiation generates disorder whilst for N<sup>+</sup> implantation damaged substrates He<sup>+</sup> irradiation anneals disorder. Possible mechanisms to account for this behaviour are discussed and the potential problems associated with accurate disorder measurements using RBS/channelling outlined.

INTRODUCTION

Rutherford backscattering/channelling analysis using MeV He<sup>+</sup> ion beam probes is a common technique for disorder assessment in semiconductors<sup>1</sup>. It is known, however, that the technique is perturbational and is generally unable to assess, for this and other fundamental reasons, disorder densities less than about 1% total lattice randomisation. Two of the important perturbational processes are:

- 1) the generation of disorder by the He probe additional to that which may already exist in the substrate, and
- 2) the annealing of disorder, which may already exist in the substrate, by the He probe.

The first process has been studied in some detail recently for Si<sup>2,3,4,5</sup> since the effect is far stronger near the surface than would be expected from

the usual modified<sup>6</sup> Kinchin-Pease<sup>7</sup> damage generation model. Investigations<sup>8</sup> with GaAs have also revealed the higher than expected disorder production rate and, in addition, have suggested that the disorder generated by the He probe is non-linearly additive to that created by a previous heavier ion irradiation. The second process was noted in Si<sup>9,10,11</sup> and GaAs<sup>12</sup> and more recently annealing<sup>13</sup> of Si<sup>+</sup> implanted Si on sapphire has been reported at temperatures from 200°C to 400°C using He<sup>+</sup>, N<sup>+</sup> and Ne<sup>+</sup> ions in the hundreds of keV range. Early studies with Te<sup>+</sup> implanted GaP<sup>14</sup> revealed no measurable annealing with 1 MeV He<sup>+</sup> ions (indeed the increased disordering process was noted) nor with 10 keV or 15 keV He<sup>+</sup> ions which should possess defect generation depth profiles overlapping the Te<sup>+</sup> disorder profile.

As part of a programme of investigation of heavy ion disorder production in InP<sup>15</sup> using He<sup>+</sup> ion backscattering analysis we have observed the operation of both disordering and annealing processes with some rather unusual and unexpected results which will be presented and discussed in this communication.

#### EXPERIMENTAL

Full details of the experimental technique have been given elsewhere<sup>15</sup> and only a brief summary, relevant to the present study, will be given here. Commercially prepared (100) InP samples were bombarded at room temperature with 40 keV N<sup>+</sup> ions to fluences of  $10^{13} \text{ cm}^{-2}$ ,  $3 \times 10^{13} \text{ cm}^{-2}$ ,  $10^{14} \text{ cm}^{-2}$ ,  $10^{15} \text{ cm}^{-2}$  and  $5 \times 10^{15} \text{ cm}^{-2}$  at fixed dose rate of  $1 \mu\text{a cm}^{-2}$ . This latter parameter was controlled since it is known to influence the amount of disorder produced and retained in the InP<sup>15</sup>. The samples were tilted  $\sim 7^\circ$  from normal incidence to minimise N<sup>+</sup> ion channelling effects.

After implantation the damage induced in the InP was analysed by Rutherford scattering/channelling studies using 2 MeV He<sup>+</sup> ions in random or (100) aligned incidence, 168° scattering angle geometry.

Backscattering spectra for aligned incidence were determined as a function of incident He<sup>+</sup> integrated ion charge up to ~50 μC (equivalent to a He<sup>+</sup> ion fluence density of ~3 x 10<sup>16</sup> cm<sup>-2</sup>). The minimum charge required for good statistical evaluation of disorder was approximately 1.5 μC. In subsequent evaluation of the measured data, the backscattering yield spectra for given integrated charge were normalised to the equivalent values for a 1.5 μC integrated charge. He<sup>+</sup> ion currents of 4.5 nA were generally employed (over an area of ~1 mm<sup>2</sup>) but some studies were conducted with 25 nA ion currents.

In addition to use of the He<sup>+</sup> ion probe for analysing N<sup>+</sup> implant induced disorder, studies were also made of the effects of He<sup>+</sup> probe beams on non-implanted samples in which the same strategy as above was followed but with an unimplanted InP crystal.

## RESULTS

Figure 1 shows backscattering/channelling spectra from non-implanted InP normalised to expected yields for 1.5 μC integrated charge as a function of increasing He<sup>+</sup> ion charge (fluence). Only the portion of the spectrum in the region of backscattering from displaced In atoms is displayed since backscattering yields from the lighter mass P are much lower and difficult to determine accurately against the rising dechannelling background at lower scattering energies<sup>15</sup>. It is clear that, for this initially undamaged substrate, the He<sup>+</sup> probe ion generates In displacements at all depths, but

in particular, near the surface where a low initial level of In displacements already exists. The increase in this In disorder is determined from the integrated area of the peaks in Figure 1 with normal linear dechannelling corrections applied<sup>16</sup>. An effective cross-section for disordering may be deduced from the initial slope of a linear or semi-logarithmic plot of In disorder as a function of fluence from the relation<sup>3</sup>:

$$\sigma_d = \frac{1}{N_0} \frac{dN_d}{d\phi} \approx \frac{d(\log N_d)}{d\phi} \quad (1)$$

where  $N_0$  is the initial area of the surface peak and  $\frac{dN_d}{d\phi}$  is the slope of the increase in surface peak area with respect to fluence plot. Determination of this value from the data of Figure 1 yields  $\sigma_d \approx 2.5 \times 10^{-17} \text{ cm}^2 \text{ ion}^{-1}$ . This value is a factor of about four larger than cross-sections measured at 40 K and 300 K for 1 MeV  $\text{He}^+$  irradiation of Si<sup>5</sup>, but rather similar to cross-sections measured<sup>8</sup> at 50 K for 2 MeV  $\text{He}^+$  irradiation of GaAs.

This value of  $\sigma_d$  for InP must however be regarded as an upper limit since after the first 4-5  $\mu\text{C}$  integrated  $\text{He}^+$  probe charge there is little further change in the area of the surface peak once the dechannelling correction has been applied. Moreover repetition of the experiment, but with lower initial,  $\text{He}^+$  fluences showed an initial negative value of  $\sigma_d$  (i.e. an annealing occurred), with a cross-section of order  $10^{-15} \text{ cm}^2$ . For  $\text{He}^+$  fluences greater than about  $5 \times 10^{14} \text{ cm}^{-2}$  the process changed to a disordering mechanism with a cross-section  $\sigma_d$  similar to the value indicated above, but again at still higher fluences ( $>10^{15} \text{ cm}^{-2}$ ),  $\sigma_d$  tended towards zero.

The concurrent studies<sup>15</sup> of heavier ( $\text{N}^+$  and  $\text{Bi}^+$ ) ion implantation into InP have shown that with increasing 40 keV  $\text{N}^+$  ion fluences the total In disorder increases rapidly in the fluence range  $10^{13} \text{ cm}^{-2}$  to about  $3 \times 10^{14} \text{ cm}^{-2}$  and then much more slowly with increasing fluence. The RBS/channelling data reveal that in the lower fluence regime the In peak does not reach the random level (i.e. the near surface region is disordered but apparently not fully randomised) but at higher fluences the In peak reaches the random level and then continues to broaden. In common with earlier interpretations for other

amorphised over a small depth near the surface and, as fluence is further increased the amorphised layer thickness increases. As a result of this data,  $N^+$  ion fluences were implanted to correspond to disorder levels from  $\sim 10\%$  initial randomisation, through initial randomisation and beyond this level to where the randomised layer thickness was increasing slowly with fluence. This required ion fluence densities to be chosen from  $10^{13} \text{ cm}^{-2}$  to  $5 \times 10^{15} \text{ cm}^{-2}$  as indicated earlier. Following each of these  $N^+$  implants the InP was analysed with 2 MeV  $\text{He}^+$  ions under aligned conditions and the backscattering data determined for increasing He fluence. Examples of the results of these analyses are shown in Figures 2, 3 and 4 for initial  $N^+$  ion implant fluences of  $10^{14}$ ,  $10^{15}$  and  $5 \times 10^{15} \text{ cm}^{-2}$  which correspond to situations of less than initial randomisation, the region of layer randomisation and of randomised layer thickening respectively. These figures all indicate that, with increasing He irradiation the number of displaced In atoms in the near surface peak is decreased. For the two lower  $N^+$  implant fluences there is also a decrease in the  $\chi_{\text{min}}$  behind the In peak and a decrease in the deeper dechannelling level. In the case of the highest fluence  $N^+$  implant there is an increase in  $\chi_{\text{min}}$  and deeper dechannelling accompanying (as in the lower  $N^+$  fluence cases) a reduction in the In peak height. In Figures 2 and 3, there is clearly a narrowing of the In peak also from the deeper side of the peak (the apparent shift of the surface side of the peak for the  $10^{15} \text{ cm}^{-2}$  may well be due to a small shift in the energy scale for one particular analysis after 15  $\mu\text{C}$ ), whereas there is no clear inward shift or peak narrowing for the  $5 \times 10^{15} \text{ cm}^{-2}$   $N^+$  implant condition. When, however, it is remembered that the dechannelling increases with  $\text{He}^+$  ion fluence in this case then when the dechannelling subtraction is made from the peak region, the deep edge of the peak does indeed move towards the surface and the peak narrows.

All of the above experiments were repeated several times with essentially qualitatively similar results although the magnitudes of the effects varied slightly. Very similar results were obtained with  $\text{He}^+$  ion probe currents of 4.5 nA and 25 nA and the results of Figure 4 were also repeated when, following data acquisition for 15  $\mu\text{C}$   $\text{He}^+$  collected charge, the counters were cleared and an analysis performed for a further 1.5  $\mu\text{C}$  collected charge. Dead time

magnitude of the effect.

Figures 2, 3 and 4 all demonstrate that the effect of the He<sup>+</sup> ion probe is, for all levels of N<sup>+</sup> implantation induced disorder, to induce an annealing behaviour. In the same way as a He<sup>+</sup> ion disordering cross-section was determined, it is possible to deduce an annealing cross-section

$$\sigma_a = - \frac{1}{N_{d_i}} \frac{dN_d}{d\phi} \tag{2}$$

where N<sub>d<sub>i</sub></sub> is the initial level of N<sup>+</sup> induced disorder.

Evaluation of σ<sub>a</sub> from the data of Figures 2, 3 and 4 yields a value of 1 → 2 x 10<sup>-17</sup> cm<sup>2</sup> ion<sup>-1</sup>. This value of σ<sub>a</sub> was relatively independent of N<sub>d<sub>i</sub></sub> from ~10% randomisation to above initial randomisation and did not appear to vary substantially with increasing He<sup>+</sup> ion fluence. In the case of N<sup>+</sup> implanted GaAs at 40 K<sup>8</sup> the effect of the He<sup>+</sup> probe was to increase the disorder with a cross-section σ<sub>d</sub> which was relatively independent of N<sub>d<sub>i</sub></sub>.

In addition to these measures of cross-section, estimates may also be made of cross-sections from the increase or decrease of the dechannelling minimum χ<sub>m</sub> immediately behind the surface peaks from a formalism equivalent to equations (1) and (2), i.e.

$$\sigma_d(\chi_m) = \pm \frac{1}{\chi_{m_o_i}} \frac{d\chi_m}{d\phi} \tag{3}$$

Deduction of these σ values from Figures 1 to 4 yields:

$$\sigma_d(\chi_m) \approx 6 \times 10^{-17} \text{ cm}^2 \text{ ion}^{-1} \text{ for unimplanted InP}$$

$$\sigma_a(\chi_m) \approx 1.4 \times 10^{-17} \text{ cm}^2 \text{ ion}^{-1} \text{ for N}^+ \text{ implanted InP for fluences up to about } 10^{15} \text{ cm}^{-2}.$$

and

$$\sigma_d(\chi_m) \approx 3 \times 10^{-18} \text{ cm}^2 \text{ ion}^{-1} \text{ for } N^+ \text{ implanted InP for a fluence of } 5 \times 10^{15} \text{ cm}^{-2}.$$

#### DISCUSSION

Considering first the disordering induced by  $\text{He}^+$  irradiation of unimplanted InP it is noted that the cross-sections for Si, GaAs and InP are all of similar order. This, as has been argued elsewhere<sup>3-5</sup>, is always substantially larger than would be expected from calculations of damage production cross-sections based upon Kinchin-Pease<sup>7</sup> calculations which account for recoil multiplication processes in addition to direct He-In collisions. This phenomenon is not well understood but may result from lower than bulk value displacement energies for near surface atoms<sup>5</sup> and from relaxed atoms around displacements contributing to He backscattering<sup>3,17</sup>. There is some evidence for the latter or similar processes in the present data.

If scattering occurs only from fully displaced atoms then, as shown by Bøgh<sup>18</sup>,  $\chi_m$  should be linearly related to  $N_d$ . This relationship has been well demonstrated for heavier than He ion implantation of Si<sup>19</sup>, GaAs<sup>20</sup> and InP<sup>21</sup> irradiated at low temperature. The present data which indicate  $\sigma_{\chi_m} \approx 2.5 \sigma_d$  suggest a relationship of the form  $\chi_m = kN_d^{2.5}$ . The earlier studies of 1 MeV  $\text{He}^+$  irradiated Si<sup>5</sup> at 40 K also suggest a slightly superlinear relationship between  $\chi_m$  and  $N_d$  whilst measurements with heavier ion implanted Si<sup>5</sup> at 40 K indicate a slight superlinearity for  $\text{P}^+$  implantation.

All of these results suggest that strain effects are also contributing to the measured dechannelling process. These may result from atomic relaxations



around completely displaced atoms (and vacancies) and from defect clusters which may form in the present studies at room temperature where, our parallel studies with heavier implant ions/<sup>15</sup> suggest considerable defect migration must occur.

Turning now to the  $\text{He}^+$  probe annealing effects in already  $\text{N}^+$  implant damaged InP it is notable that, for all disorder levels,  $\sigma_a$  is considerably smaller than  $\sigma_d$  but for the highest disorder level although annealing of the peak disorder occurs, there is a simultaneous disorder production as evidenced by the increase in  $\chi_m$  with  $\text{He}^+$  fluence (i.e.  $\sigma_d$  is positive). Moreover whilst it is true that some of the peak annealing occurs by apparent regrowth of the "amorphous" layer from the crystalline substrate as evidenced by the shift towards the surface of the inner boundary of the peak, it is also clear that annealing occurs within this "amorphous" layer itself since the peak height is everywhere continuously reduced by increasing  $\text{He}^+$  irradiation.

The mechanisms responsible for this unusual behaviour are currently unclear but seem not to be associated simply with thermal reordering within the randomised layer and at the random-crystal interface since changes in  $\text{He}^+$  beam power by a factor of 5 resulted in no notable differences in anneal behaviour. We speculate, however, that although the RBS/channelling data reaches the random level that this is not a precise indicator of full amorphisation and that the near surface region may be either totally microcrystalline or largely amorphous with small included crystalline regions. If either were the case then some recrystallisation in this layer would be possible by  $\text{He}^+$  induced defect generation and migration and/or by inelastic energy loss processes which disrupt the rearranged bonding configuration created by implantation. We propose to further investigate these processes by variation of probe energy, and species in order to vary elastic and inelastic energy loss rates as has been initiated with GaAs.<sup>8</sup> If such local reordering does in fact occur than it may partly account for the positive

$\sigma_d(\chi_m)$  observed for initially heavily disordered layers since such crystallite zones and their environs could lead to local strains and enhancement of dechannelling. It is also clear that microscopic (TEM) and low incidence angle diffraction techniques would be helpful in obtaining a clearer understanding of the nature of the near surface damaged layer.

It is thus believed, in common with earlier suggestions<sup>9-13</sup>, that the  $\text{He}^+$  probe annealing process is due to simple defect production which interacts with the more stable initial disorder and reduces and modifies this disorder.

Finally the present results indicate a problem which has not arisen previously in the  $\text{He}^+$  probe analysis of Si and GaAs. In these materials it has been noted that the  $\text{He}^+$  probe always creates additional disorder to that induced by implantation and even if these disorders are non-linearly additive<sup>8</sup> the  $\text{He}^+$  probe effect can be described by a more or less constant production cross-section process. Appropriate deconvolution of measured disorder data to give actual disorder data can then be made<sup>5,8</sup>. In the case of InP it appears that for disorder levels somewhere, as yet poorly specified, between 1% and 10% initial randomisation,  $\sigma$  probably changes sign. At high disorder levels, and since  $\text{He}^+$  probe fluences necessary for analysis are generally low, the sign and low magnitude of  $\sigma$  result in little adjustment to be made to measured data to recover actual disorder data. Such adjustments are much more severe in the low implant fluence (low disorder concentration) regimes where, as just noted  $\sigma$  values are poorly described in sign and magnitude. Thus the accurate evaluation of low disorder concentrations in InP is much poorer than either Si and GaAs. At a fundamental level the variation of  $\sigma$  with increasing disorder  $N_d$  can be explained in terms of a disorder production cross-section  $\sigma_d$  which decreases with  $N_d$  and a competing disorder annealing cross-section  $\sigma_a$  which either increases or remains constant with increasing  $N_d$ . Evidence for some competitive effect exists from the data of Figure 4 discussed earlier

which reveals both a  $\sigma_a$  component in the disorder peak annealing and a  $\sigma_d(\chi_m)$  component in the dechannelling increase. Again we can only speculate on the reason for this behaviour at present. Thus for an unimplanted substrate  $N_{d_0}$  may represent In atoms in either or both a relaxed state due to surface proximity and in a surface oxide. After implantation  $N_{d_i}$  represents In atoms displaced and partly relaxed from lattice sites as a result of the implantation induced collision cascades. The interaction of the He beam with these different configurations of In atoms, and indeed P atoms, may well be responsible for the observations together with processes which may be non-linear in  $N_d$  such as defect migration and annihilation with existing defects which will increase in importance with increasing  $N_d$ . It is quite clear that further studies of these disordering and annealing processes induced by  $\text{He}^+$  (and other probe) species following a variety of ion implant conditions are necessary in order to optimally employ RBS/channelling as an implant disorder analysis tool with InP.

#### REFERENCES

1. W K Chu, J W Mayer and M A Nicolet. "Backscattering Spectrometry". (Academic Press, New York) 1978.
2. W H Kool, H E Roosendaal, L W Wiggers and F W Saris. Nucl Instrum & Meth 132, 285 (1976).
3. W H Kool, H E Roosendaal, L W Wiggers and F W Saris. Rad Effects 36, 41 (1978).
4. L W Wiggers, H G Koekkoek, A H Buth, F W Saris and H E Roosendaal. Rad Effects 42, 77 (1979).
5. D A Thompson, G Carter, H K Haugen and D V Stevanovic. Rad Effects 46, 71 (1980).
6. P Sigmund. Appl Phys Letters 25, 169 (1974).

7. G H Kinchin and R S Pease. Rep Prog Phys 18, 143 (1955).
8. D V Stevanovic, N P Tognetti, G Carter, C E Christodoulides, A M Ibrahim and D A Thompson. Rad Effects. To be published, 1982.
9. S T Picraux and F L Vook. Rad Effects 11, 179 (1971).
10. E Bøgh, P Høgild and I Stensgaard. Rad Effects 7, 115 (1971).
11. J K Hirvonen, W L Brown and P M Glotin. 2nd Int Conf on Ion Implantation in Semiconductors (Eds I Ruge and J Graul, Springer-Verlag, Berlin) p8 (1971).
12. J S Harris. 2nd Int Conf on Ion Implantation in Semiconductors (Eds I Ruge and J Graul, Springer-Verlag, Berlin) (1971).
13. B Svensson, J Linnros and G Holmen. Proc 2nd Int Conf on Ion Beam Modification of Materials, Grenoble, 1982. To be published in Nucl Instrum and Meth, 1983.
14. G Carter and J L Whitton. Rad Effects 15, 143 (1972).
15. Zhang Tong He, G Carter and R G Elliman. 2nd Int Conf on Ion Beam Modification of Materials, Grenoble, 1982. To be published in Nucl Instrum and Meth, 1983.
16. J S Ziegler and W K Chu. Atomic and Nuclear Data Tables 13, 35 (1978).
17. H H Hubbes, B Schmedeskamp, H E Roosendaal and H O Lutz. To be published.
18. E Bøgh. Can J Phys 46, 653 (1968).
19. R S Walker, D A Thompson and S W Poehlman. Rad Effects 34, 157 (1977).
20. N P Tognetti. Rad Effects Letters 58, 151 (1981).
21. R G Elliman. Rad Effects Letters. To be published, 1983.

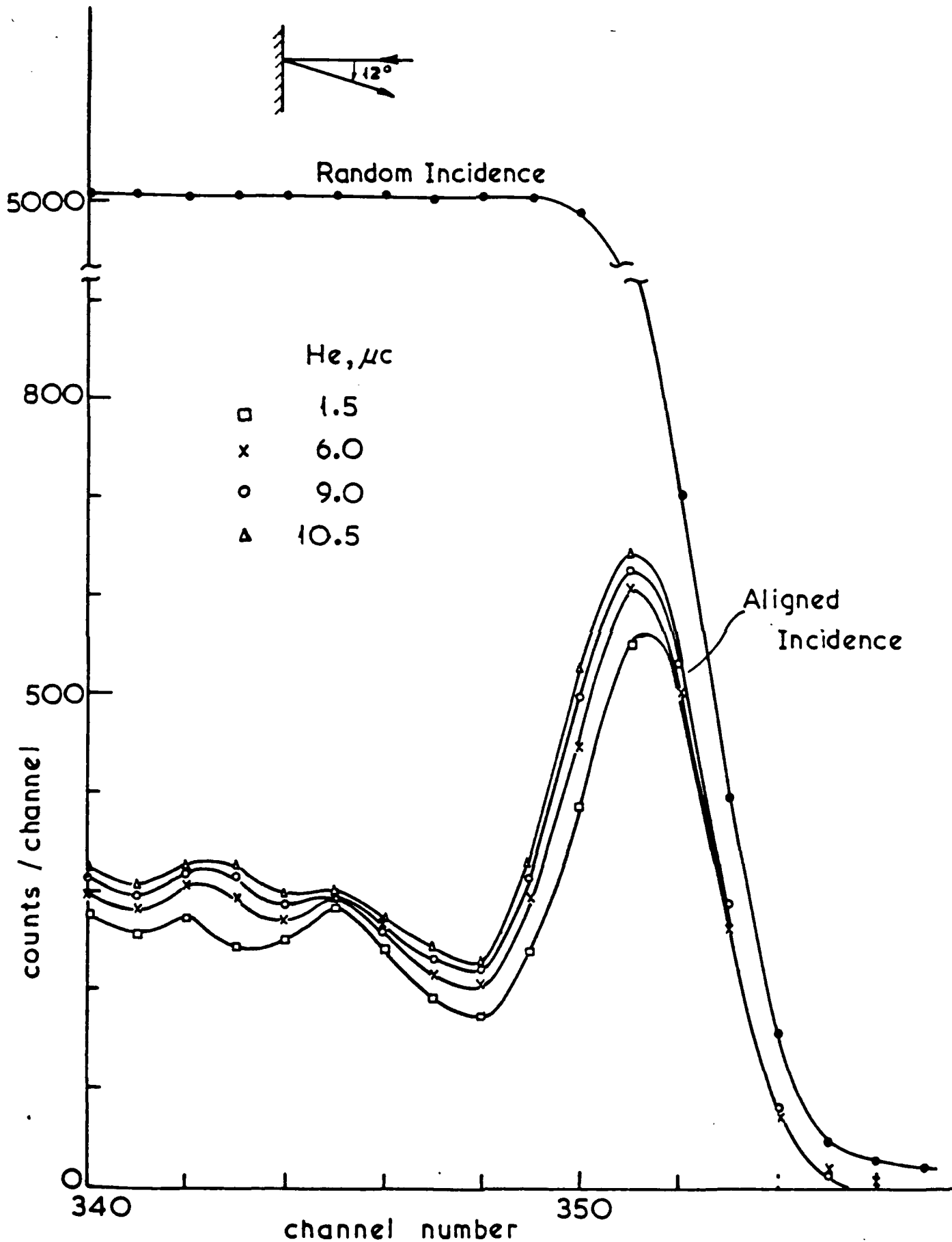


Fig 1 Rutherford backscattering/channelling spectra of random and  $\langle 100 \rangle$  aligned incidence 2MeV  $\text{He}^+$  ions from In atoms in an unimplanted InP substrate as a function of He ion flux

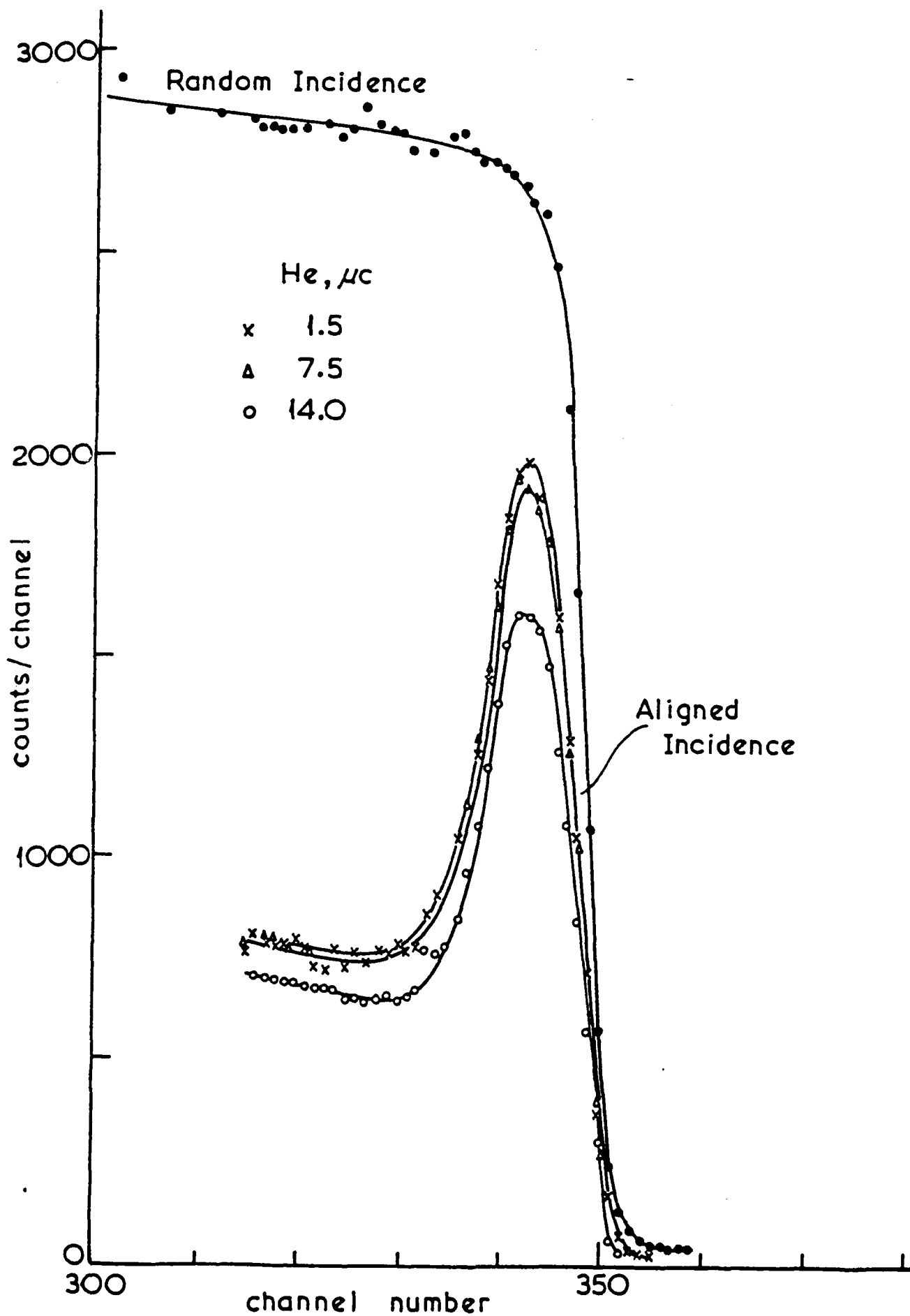


Fig. 2 Rutherford backscattering/channelling spectra of random and  $\langle 100 \rangle$  aligned incidence 2 MeV  $\text{He}^+$  ions from In atoms in an InP substrate implanted with  $40 \text{ keV } 10^{14} \text{ N}^+$  ions  $\text{cm}^{-2}$  as a function

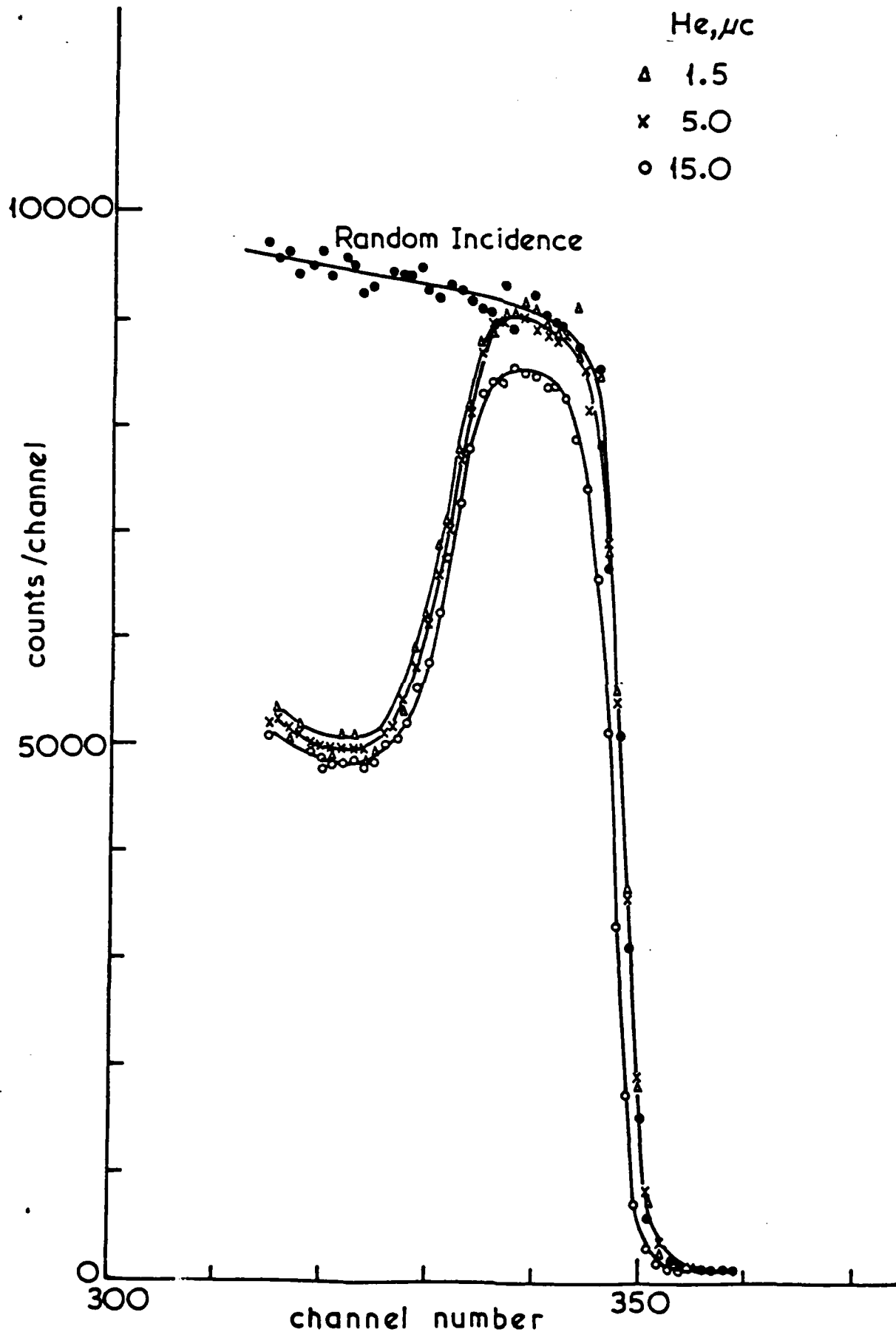


Fig. 3 Rutherford backscattering/channelling spectra of random and  $\langle 100 \rangle$ -aligned incidence 2 MeV  $\text{He}^+$  ions from In atoms in an InP substrate implanted with 40 keV  $10^{15} \text{N}^+$  ions  $\text{cm}^{-2}$  as a function

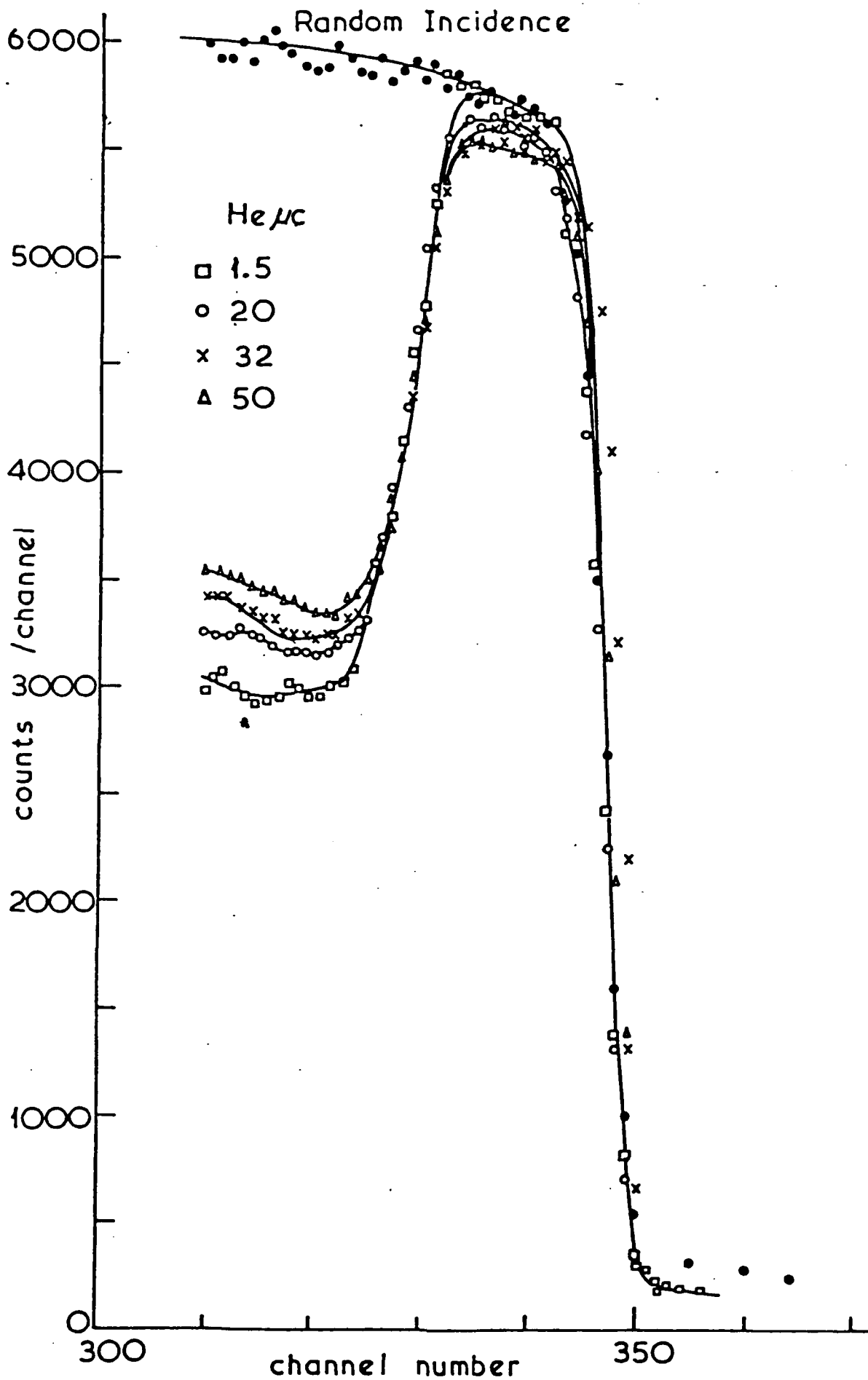


Fig.4 Rutherford backscattering/channelling spectra of random and  $\langle 100 \rangle$  aligned incidence 2MeV  $\text{He}^+$  ions from In atoms in an substrate implanted with 40keV  $5 \times 10^{15} \text{N}^+$  ions  $\text{cm}^{-2}$  as a function



### General Conclusions

Over the period of the grant award the investigators at Salford have undertaken two functions. Firstly an analytical assessment of samples provided by the sponsor at Wright Patterson AFB have been undertaken to the sponsors requirements. The results of this work were described in our earlier report and not only reveal problems associated with strain at silicon on sapphire interface structures but also suggested further studies which could be performed at Wright Patterson.

Secondly an associated research programme on ion implantation processes in Si, GaAs and more recently InP has been undertaken to provide basic intelligence to the potential application of the ion implantation technique in device construction relevant to the interests of the sponsor. The results of these studies have been documented in the earlier and present, final reports. It is believed that considerable new understanding of the fundamental processes of damage creation attendant upon ion implantation of these semiconductor materials, and upon impurity incorporation during furnace annealing of Si, has been achieved. This is beneficial, not only to the grant sponsor and the University investigators, but to the international scientific and technological community concerned with the use of ion implantation in the present and potential applications to semiconductor device production. The University investigators express gratitude to the USAF for provision of the financial support which has enabled prosecution of these investigations.

END

11-86

DT/C